[AMERICAN JOURNAL OF SCIENCE, VOL. 299, JUNE, 1999, P. 467–501]

# POROSITY EVOLUTION AND MINERAL PARAGENESIS DURING LOW-GRADE METAMORPHISM OF BASALTIC LAVAS AT TEIGARHORN, EASTERN ICELAND

PHILIP S. NEUHOFF*, THRÁINN FRIDRIKSSON*, STEFÁN ARNÓRSSON**, and DENNIS K. BIRD*

**ABSTRACT. Low-grade alteration of basaltic lavas at Teigarhorn, eastern Iceland, resulted in three distinct stages of mineral paragenesis that correlate to events in the burial and intrusive history of Icelandic crust. Metasomatism and brittle deformation during the paragenetic stages dramatically affected the paleohydrology of the lavas and formed temporally distinct mineral assemblages. The lavas initially contained up to 22 percent total porosity concentrated near the tops and bottoms of individual lava flows. Celadonite and silica (Stage I) precipitated along the walls of primary pores prior to deep burial of the lavas and occluded ~8 percent of the initial porosity. During burial (Stage II), hydrolysis of olivine and basaltic glass led to the formation of mixed-layer chlorite/smectite clays in the matrix of the lavas and as rims filling ~40 percent of the volume of primary pores. Chlorite contents in Stage II mixed-layer clay rims increased from ~20 to ~80 percent during the infilling of individual vesicles, reflecting increasing temperatures with time as the lavas were buried. The end of Stage II occurred after burial and is represented by filling of ~40 percent of total primary porosity by zeolites (scolecite or heulandite + stilbite + mordenite ± epistilbite) and replacement of plagioclase by zeolites and albite. The Stage II zeolite assemblages are indicative of two regional metamorphic mineral zones in eastern Iceland, the mesolite + scolecite and heulandite + stilbite zones. The presence of the boundary between the mesolite + scolecite + and heulandite + stilbite zones indicates that the maximum temperature during burial metamorphism was 90° ± 10°C. Localized areas of intense hydrothermal alteration associated with intrusion of basaltic dikes (Stage III) overprint Stages I and II. Extensive fracturing and hydrothermal brecciation during Stage III added 3 to 11 percent total porosity in which mm- to cm-scale museum-grade crystals of quartz, calcite (Iceland spar), stilbite, scolecite, heulandite, and laumontite precipitated. Estimates of the temperature during Stage III (based on fluid inclusion homogenization temperatures in calcite, chlorite geothermometry, and the zeolite assemblage) range from 120° to 180°C. Although the thermobarometric conditions during Stages II and III led to similar mineral assemblages, careful attention to textural and geologic relations permits seemingly complex, multi-stage parageneses in metabasalts to be interpreted in a petrotectonic context.**

## INTRODUCTION

The mineralogy of low-grade metabasalts is a sensitive indicator of the thermobarometric evolution of oceanic crust and continental flood basalts. Discrete temperature-, pressure-, and/or depth-controlled zones characterized by assemblages of silica minerals, phyllosilicates, and zeolites frequently serve as metamorphic indicators in low-grade metabasalts. Zones containing trioctahedral smectite, corrensite and/or mixed layer chlorite/smectite, and chlorite occur with increasing metamorphic grade in zeolite- and greenschist-facies metabasalts and active geothermal systems in basaltic rocks (Mehegan, Robinson, and Delany, 1982; Seki and others, 1983; Liou and others, 1985; Bevins, Robinson, and Rowbotham, 1991; Robinson, Bevins, and Rowbotham, 1993; Schmidt, 1990; Schmidt and Robinson, 1997; Kristmannsdóttir, 1979; Schiffman and Fridleifsson, 1991; Robinson and Bevins, 1999; Alt, 1999). In addition, as many as five separate depth-controlled "zeolite zones" have been described in regionally metamorphosed basaltic lavas and Icelandic geothermal systems (Walker, 1951, 1960a,b; Sukheswala,

* Department of Geological and Environmental Science, Stanford University, Stanford, California 94305-2115

** Science Institute, University of Iceland, Dunhagi 3, 107 Reykjavik, Iceland

Avasia, and Gangopadhyay, 1974; Kristmannsdóttir and Tómasson, 1978; Jørgensen, 1984; Murata, Formoso, and Roisenberg, 1987; Schmidt, 1990; Neuhoff and others, 1997; Christiansen and others, 1999). Phyllosilicate and zeolite parageneses thus provide useful information for evaluating heat flow and structural evolution in large igneous provinces (Neuhoff and others, 1997) and exploration potential in fractured basaltic petroleum reservoirs (Christiansen and others, 1999). Complicating such interpretations, however, is the fact that basaltic provinces often undergo multiple stages of intrusion, extrusion, and deformation during which the lavas are altered through weathering, regional burial metamorphism, and local hydrothermal/contact metamorphism. Mineral assemblages formed during regional metamorphism and localized hydrothermal alteration can be nearly identical, complicating interpretation of mineral isograds associated with burial metamorphism (Neuhoff and others, 1997; Sukheswala, Avasia, and Gangopadhyay, 1974).

In the present study, we demonstrate that regional and local mineral parageneses in low-grade metabasalts can be distinguished on the basis of geologic and textural relations. These relations are difficult to establish from drillcores and areas of limited outcrop. Ideally one would like to investigate the textural and geologic relations between mineral parageneses in laterally continuous, unweathered outcrop exposures. Remarkable outcrop exposures created through coastal erosion at Teigarhorn, eastern Iceland (fig. 1), permit such detailed observations of geologic and textural relationships in basaltic lavas affected by burial metamorphism, brittle deformation, and hydrothermal alteration during dike emplacement. Geologic, petrographic, mineral chemical, and hydrologic information based on field and laboratory studies are presented in order to distinguish mineral assemblages and textures associated with three paragenetic stages of alteration at Teigarhorn: syn-eruptive, near surface alteration (Stage I), regional burial metamorphism (Stage II), and local hydrothermal alteration associated with dike emplacement (Stage III). Each stage is characterized by distinct mineral parageneses and textures, with Stage II resulting in formation of the regional zeolite zones described by Walker (1960b). Bulk porosity varied considerably during the metamorphic history of the lavas due to filling of pore spaces by secondary minerals and generation of secondary porosity through brittle deformation. The results provide an example of how observations of mineral paragenesis and porosity evolution can be integrated in a petrotectonic interpretation of low-grade metamorphism in basaltic terraines.

## GEOLOGICAL SETTING

*Geology*.–Teigarhorn is located near the eastern edge of the volcanic plateau of present-day Iceland (fig. 1). Lavas erupted from fissures and central volcanoes during magmatism along a divergent plate boundary between the North American and Eurasian plates (Kristjánsson, Gudmundsson, and Haraldsson, 1995). The oldest exposed lavas are only about 13 Ma (Watkins and Walker, 1977). Upper crustal stratigraphy in eastern Iceland consists largely of subaerial basaltic lavas with minor intercalated sediments, silicic lavas, lignite layers, and pyroclastic units (Robinson and others, 1982; Gústafsson, 1992; Walker, 1960b; Wood, 1977; Sæmundsson, 1979). Continued volcanism and rifting led to pronounced tilting of the lavas that dominate crustal structure around Teigarhorn (Pálmason, 1973); dips increase from $<2°$ to 6° southwest at the top of the lava pile to $\sim 6°$ to 9° southwest at sealevel (fig. 1; Walker, 1974).

Disrupting the monoclinal structure of the lava pile are mafic and silicic intrusive centers and central volcanic complexes (fig. 1; Walker, 1963). Extrusive products of the extinct central volcanoes are interlayered with fissure-erupted lavas that make up most of the crust in eastern Iceland. Glacial exhumation has revealed an alignment of mafic dice swarms, central volcanoes, and intrusive centers that defines the geometry of paleo-rift zones. Teigarhorn lies within a prominent dike swarm (called the Álftafjördur dike

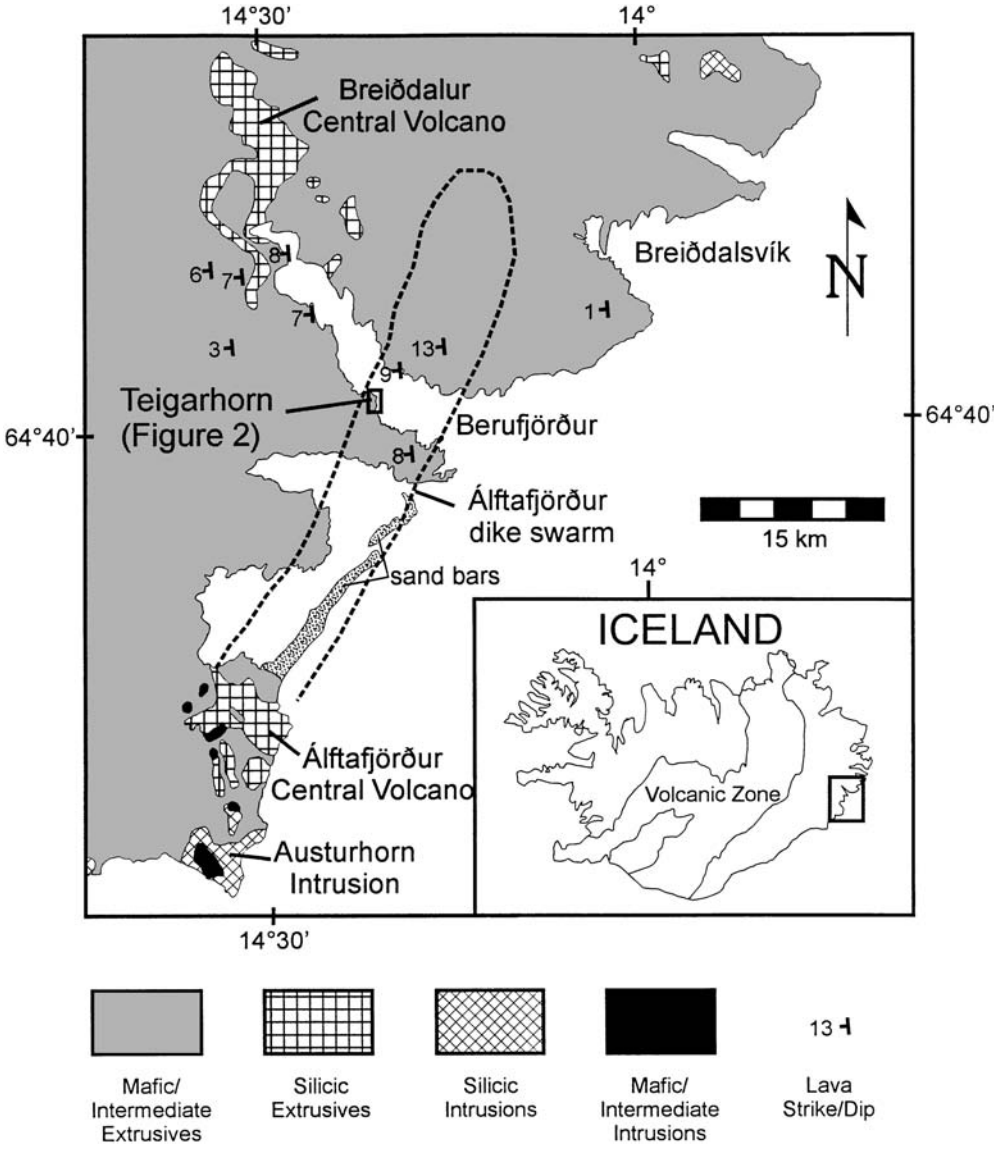


Fig. 1. Generalized geological map of a portion of eastern Iceland (after Jóhannesson and Sæmundsson, 1989) showing the distribution of major rock types, locations of intrusions and central volcanoes, and selected lava orientations from Walker (1963, 1974). Dashed curve outlines the Alftafjördur mafic dike swarm where dikes make up greater than 8 percent (by volume) of the crust (Walker, 1963).

swarm; Walker, 1963): the Álftafjördur volcanic center and the Austurhorn intrusion both lie within this swarm (figs. 1 and 2; Walker, 1963; Blake, 1970). The composition and mineralogy of these dikes are similar to the surrounding basalts discussed below (Walker, 1963). The dikes are subvertical, trend north-northeast (fig. 2), and vary in thickness from 0.25 to 3 m.

*Lithology*.–The volcanic stratigraphy exposed at Teigarhorn includes approx 150 m of subaerial mafic lava flows with minor intercalated pyroclastic units. The uppermost

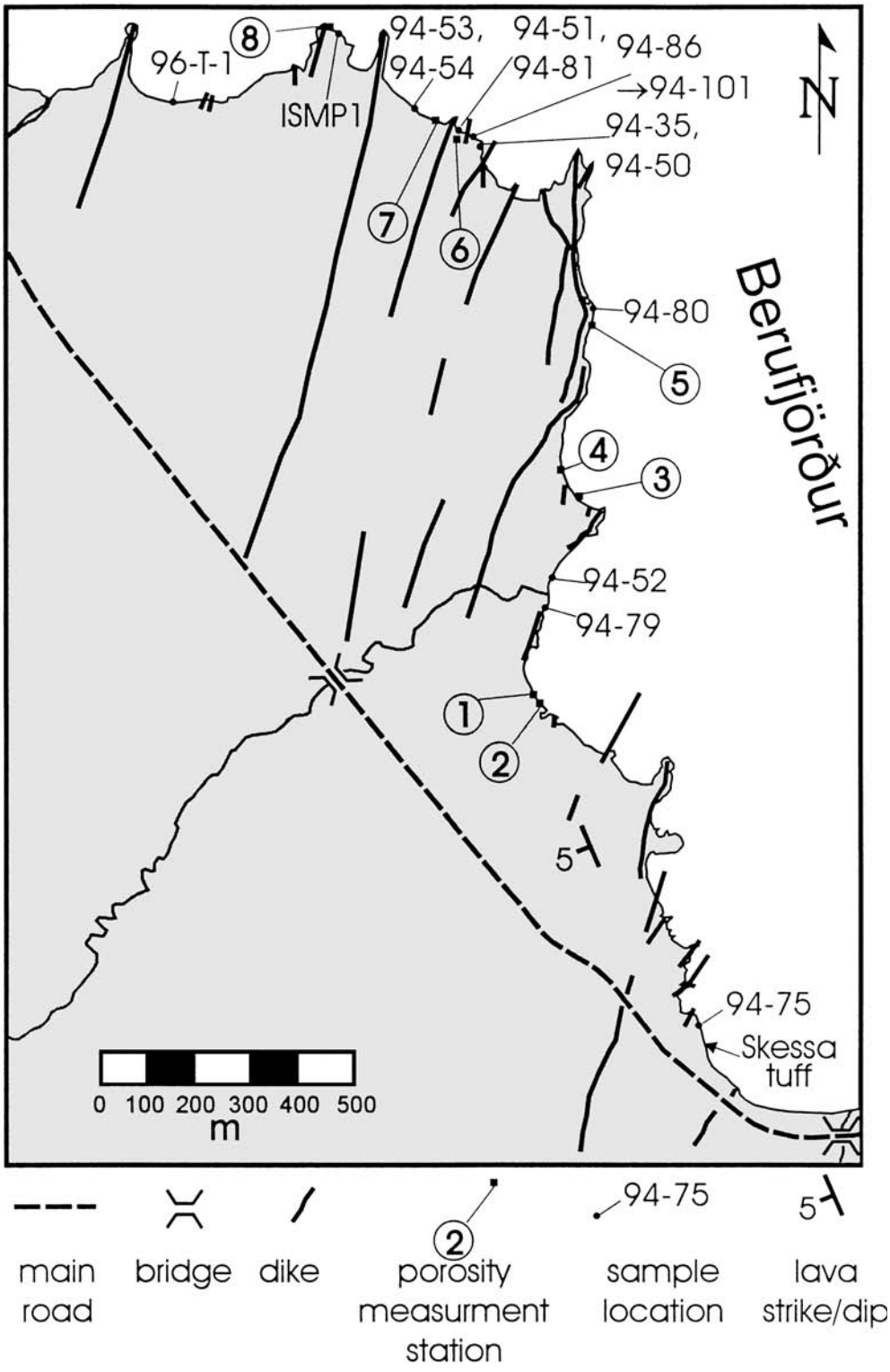


Fig. 2. Map of Teigarhorn showing the distribution of individual mafic dikes (determined by field mapping and from aerial photographs) and the locations of samples and porosity measurements. Also shown is the location of the Skessa tuff (Walker, 1963).

lavas belong to the Grænavatn Porphyritic Group (Walker, 1959), and the oldest units are the Skessa tuff (see below) and surrounding undesignated lavas. These units were buried to approx 1500m at Teigarhorn (Walker, 1960b). Compositionally, the lavas exposed at Teigarhorn (fig. 2) are 3 to 25 m thick subaerial low-MgO tholeiites and ferrobasalts (Flower and others, 1982). Most flows are fine-grained, containing abundant groundmass plagioclase, olivine, pyroxene, and glass with minor olivine and pyroxene phenocrysts. Lavas with up to 30 modal percent plagioclase phenocrysts occur infrequently. The flows have scoraceous, brecciated flow tops. Vesicles are abundant near the top and bottom of the flows, but the flow centers are essentially non-vesicular and massive. A 20 m thick, green, welded, silicic tuffaceous unit (the Skessa tuff of Walker, 1959) is exposed near the southern portion of Teigarhorn (marked "Skessa tuff" on fig. 2). The Skessa tuff is a regionally extensive unit that appears to be the product of an eruption from an unexposed volcanic center approx 25 km north of Teigarhorn (Walker, 1962). Separating many flows are undulatory weathering surfaces that frequently are overlain by bright red basaltic tephras that are 1 to 15 cm thick and constitute less than 1 percent of the stratigraphy. The tephras are phreatomagmatic deposits produced by interaction between basaltic magmas and surface or groundwaters at eruption sites 10's to 100's of km away from Teigarhorn (Heister, ms).

The volcanic stratigraphy in eastern Iceland has been subjected to regional zeolite-facies metamorphism; higher grades of metamorphism are exposed around intrusive complexes and central volcanoes (Walker, 1960b). Walker (1960b) described depth-controlled zeolite-facies mineral zones (fig. 3) that parallel the paleosurface of the lava pile and transgress the volcanic stratigraphy. This implies that the zones formed after tilting of the lava pile and do not solely reflect variations in chemistry of the host lavas. The zeolite zones described by Walker (1960b) are underlain by zones characterized by stilbite ± heulandite ± mordenite, laumontite, and prehnite + epidote with increasing depth (Mehegan, Robinson, and Delany, 1982). Coastal exposures around Berufjördur (fig. 1) have provided museum-grade zeolite specimens for over 200 yrs (Betz, 1981). Teigarhorn, in particular, has been an important source for zeolites used in studies of crystal chemistry (Galli and Rinaldi, 1974; Passaglia, 1975; Passaglia and others, 1978; Alberti, Pongiluppi, and Vezzalini, 1982), crystal structures (Slaughter and Kane, 1969), reaction kinetics (Ragnarsdóttir, 1993), optical properties (Bauer and Hrîchová, 1962), and piezoelectricity (Bellanca, 1940).

## METHODS

*Mapping and sample collection.*–Representative samples of altered and unaltered lavas were collected throughout the coastal exposures at Teigarhorn in conjunction with mapping of dike distribution and outcrop porosity measurements (fig. 2). Estimates of total macroscopic porosity (herein defined as the percentage of a given volume of rock occupied by pore space) prior to mineral precipitation were conducted in situ during mapping following the methods of Manning and Bird (1991). In the present communication, a distinction is made between the total porosity at a given point in time ($\Phi$) and the cumulative porosity that reflects pore abundance ($\Phi^*$) but does not include the effects of pore occlusion by mineral precipitation (Manning and Bird, 1991). The contribution of primary pores to $\Phi^*$ ($\Phi_1^*$) was estimated by placing a clear mylar sheet imprinted with a 54 by 41.5 cm grid (node spacing 1.5 cm) directly on the outcrop as a basis for point counting macroscopic pores. Estimates of $\Phi_1^*$ included vesicles and other primary structures as well as open space between flow units that could not texturally be linked to post-eruption processes. Although this technique only identifies macroscopic pores on the order of 1 mm or larger, the contribution of these pores to $\Phi_1^*$ is large, and uncertainties are on the order of 1.5 percent or less for grids of over 1000 points (Manning and Bird, 1991; Chayes, 1956). The contribution of secondary pore spaces to

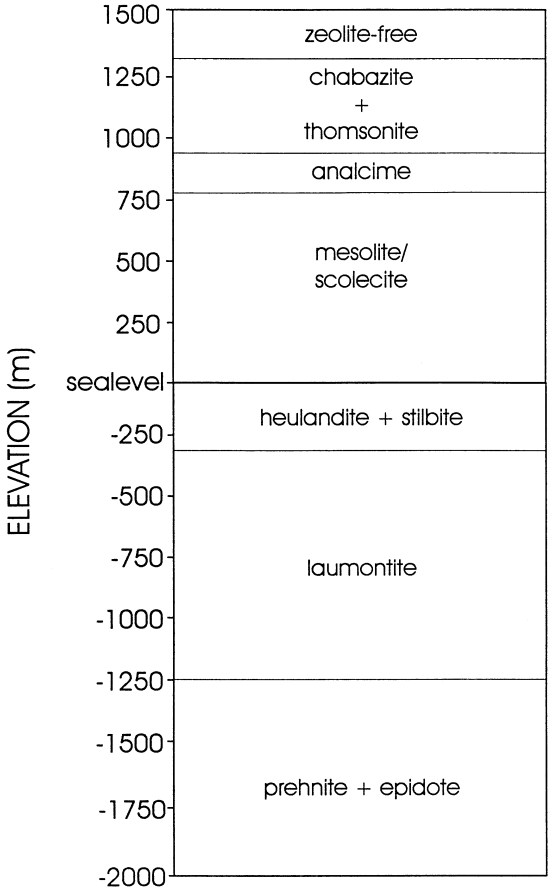


Fig. 3. Depth distribution of regional zeolite facies mineral zones in eastern Iceland. Zones above sealevel are from mapping in olivine normative tholeiites around Berufjördur by Walker (1960b) and below sealevel are from studies of the Reydarfjördur drill core located ~40 km north-northwest of Teigarhorn (Mehegan, Robinson, and Delaney, 1982). Note that the outcrops at Teigarhorn are approximately at sealevel. Stage II alteration at Teigarhorn includes both the mesolite/scolecite and heulandite + stilbite mineral zones.

$\Phi^*$ ($\Phi_2^*$) was estimated by measuring cross-sectional areas of fractures/veins, breccias, and dissolution features associated with late-stage alteration within 3 to 6 $m^2$ sections of outcrop. Although outcrop area measurements of pore space are scale dependent and not necessarily representative of bulk properties (Manning and Bird, 1991), they are useful for assessing the general magnitude and variability of $\Phi_2^*$. Repeated area measurements indicate that uncertainties were ~1 percent.

*Analytical techniques.*–Petrographic and hand-sample observations were conducted on 20 samples representative of lithologies and mineral parageneses at Teigarhorn. Optical properties of minerals in transmitted light were used along with mineral habits in both hand specimen and thin section to augment field observations of mineral parageneses and phase relations. Estimates of the percentage of pore space occupied by various alteration minerals were conducted by digital analysis of photomicrographs. Images of discrete pores were digitized using the software package Scion Image (Scion Corporation, Frederick, Maryland) to calculate the areas of various secondary phase/assemblages and residual porosity relative to the total area of the pore. Repeat measurements indicate that errors in area measurements were less than 1 percent.

A battery of analytical techniques was used to confirm phase identities and compositions. Powder X-ray Diffraction (XRD) was conducted on mineral separates using a Rigaku theta-theta diffractometer with Cu$K\alpha$ operating at 35 kV and 15 mA. Mineral separates for XRD identification were extracted from individual vesicles with a rotary drill. Mineral chemistry was determined by electron probe microanalysis (EPMA) on an automated JEOL 733A electron microprobe operated at 15 kV accelerating potential and 15 nA beam current. Calibration was conducted using natural geologic standards. Beam width for analysis of hydrous minerals (i.e., that is, clays and zeolites) was varied between 10 and 30 μm depending on grain size. Raw counts were collected for 20 s and converted to oxide wt percents using the CITZAF correction procedure after accounting for unanalyzed oxygen following the methods of Tingle and others (1996). Raw counts for individual elements (including Na) were essentially constant with time, suggesting the elemental drift (loss) was negligible. Bulk rock compositions were determined on a Rigaku fully automated X-ray fluorescence (XRF) spectrometer. Fluid inclusion homogenization and freezing temperatures were determined on one sample of calcite (Iceland spar variety) using gas-flow heating/freezing stage adapted by Fluid, Inc.

## RESULTS

### *Mineral Paragenesis*

Alteration at Teigarhorn occurred during three paragenetic stages. The textural and mineralogical characteristics of these stages are summarized in table 1 and the sequence of mineral precipitation during each stage is shown in figure 4. Representative compositions and molar formulas for clays, zeolites, and feldspars are given in tables 2 through 5.

*Stage I.*–Paragenetic stage I is the earliest alteration at Teigarhorn and is characterized by linings of primary pore space by celadonite and silica minerals (table 1; figs. 4 and 5B). All other mineral assemblages are either precipitated on top of or cross cut Stage I alteration (fig. 5B). Stage I alteration is common but not present in all samples. Celadonite and silica minerals typically form layers along the walls of pore space with a layered or botryoidal habit. Occasionally Stage I silica forms layered geopetal structures

TABLE 1

*Mineralogical and textural characteristics of paragenetic stages observed at Teigarhorn, eastern Iceland*

| Paragenetic Stage* | Mineral Assemblages in Pore Space | Mineral Assemblages in Matrix | Textures |
|---|---|---|---|
| Stage I | ±celadonite ± silica | minor celadonite | pores: lining primary pore space; geopetal structures<br>matrix: minor celadonite replacing groundmass |
| Stage II | C/S[2] + scolecite ± chalcedony ± quartz<br>C/S + stilbite + heulandite ± mordenite ± epistilbite ± qu artz ± chalcedony | C/S + albite + zeolites | pores: C/S pore linings<br>partial or complete primary pore fillings by zeolites<br>matrix: pseudomorphic replacement of groundmass and phenocrysts |
| StageIII | quartz ± clinoptilolite ± stilbite ± heulandite ± mordenit e ± scolecite ± laumontite ± calcite | quartz + C/S | pores: brecciation, fracturing, mineral precipitation<br>matrix: discoloration ($SiO_2$ metasomatism) |

*Stage I was the earliest stage, Stage III the last. [2]Mixed-layer chlorite smectite (see text).

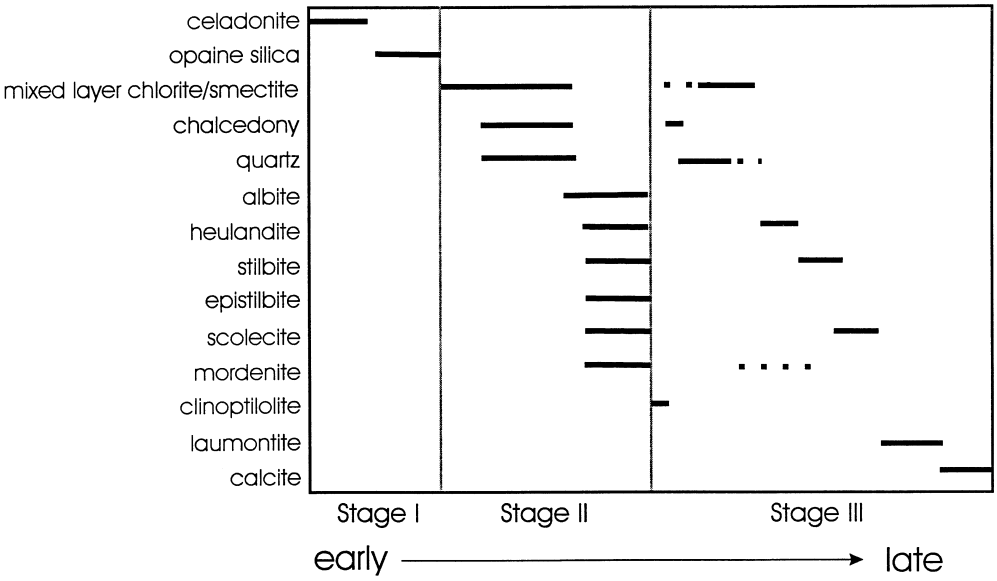


Fig. 4. Temporal sequence of secondary minerals developed in lavas at Teigarhorn. Events toward the right of the diagram occurred after events to the left.

on the bottom of vesicles that are oriented roughly parallel to the lava stratigraphy. Minor celadonite occurs in the volcanic groundmass.

Celadonite typically precedes silica in the crystallization sequence (fig. 5B). A representative celadonite composition from Teigarhorn is given in table 2, and 6 celadonite analyses are plotted in figure 6. Stage I celadonite is close to the endmember compositions as defined by Buckley and others (1978), with only slightly lower potassium content and higher aluminum than the ideal endmember composition [$K_2(Fe,Al)_2(Mg,Fe)_2Si_8O_{20}$ $(OH)_4$; table 2; fig. 6]. The slight deviation from ideal composition may be due to the presence of a small trioctahedral smectite component (either as intergrowths or interstratifications) in the celadonites, although smectite is not detected in the XRD patterns. Celadonite is distinguished from other phyllosilicates by its distinctive bright green color in both hand specimen and thin section (figs. 5B and 5D), its layered habit, and by its potassium-rich composition (table 2; fig. 6). Silica minerals consist of quartz and/or chalcedony. It appears likely that quartz and chalcedony replaced preexisting Stage I opaline silica during burial, as opaline silica is the only Stage I silica phase observed near the top of the lava pile above Teigarhorn (Neuhoff, unpublished data).

*Stage II.*–Paragenetic Stage II alteration is characterized by continued infilling of primary pore spaces and partial replacement of groundmass and phenocryst minerals. As with Stage I, the distribution at the outcrop scale of Stage II alteration is largely a function of the distribution of primary porosity in the lavas (fig. 5A). Stage II mineral assemblages and paragenetic sequences are summarized in table 1 and figure 4. Mixed layer chlorite/smectite (C/S) is the first phase to precipitate in primary pore space during Stage II (fig. 5B, C). The term "mixed layer chlorite/smectite" and the abbreviation C/S are used in the present communication without specific inference of ordering among layers (Reynolds, 1988). Brown to brownish green radiating bundles of C/S for linings of primary pore space. The bundles nucleated on pore walls or on Stage I minerals where present and developed toward the center of the pores. As shown in figure 6, Stage II C/S

compositions (table 2) project near the binary compositional join between ferromagnesian trioctahedral smectite (saponite-ferrosaponite; Güven, 1988) to ferromagnesian chlorite (clinochlore-chamosite; Bailey, 1988). The percentage of chlorite (or smectite) interlayers was estimated from electron microprobe analysis of the total molar Si + Al + Mg + Fe content of the mineral by linear interpolation between smectite and chlorite endmembers (Schiffman and Fridleifsson, 1991). This interpolation requires calculation of molar formulas based on 28 oxygen charge equivalents (O + 2OH), for which the molar Si + Al + Mg + Fe contents of endmember chlorite and trioctahedral smectite are 20 and 17.82, respectively. By this analysis, Stage II clays contain between 12 and 85 mol percent chlorite. The most prominent interlayer cations in C/S clays are $Ca^{+2}$ and $Na^{+}$ (table 2). Potassium typically accounts for less than 5 mol percent of the total interlayer cations but in rare cases constitutes more than 25 mol percent with one sample as high as 60 mol percent. Mixed-layer chlorite-smectite with high $K^{+}$ contents always occur in close proximity to celadonite, and textural evidence suggests that local replacement of Stage I celadonite by Stage II C/S may have occurred.

The compositions of C/S clays become progressively enriched in chlorite during Stage II alteration. Figure 7 shows the percentage of chlorite in a rim of Stage II C/S as a function of distance from the vesicle wall. In general, C/S near the wall of the vesicle precipitated earlier than that closer to the center of the vesicle. It can be seen in figure 7 that the chlorite content of the clay generally increases from ~20 percent at the vesicle wall to about 80 percent near the center of the vesicle, indicating that the chlorite content of Stage II C/S increased with time.

The last phases to crystallize during Stage II are minor quartz and chalcedony along with zeolites (table 1 and fig. 4) that serve as index minerals for the regional zeolite zones shown in figure 3. Zeolites partially or completely fill the pore space remaining after precipitation of C/S (fig. 5B). As indicated in table 1, two Stage II zeolite assemblages occur at Teigarhorn; the mesolite + scolecite zone described by Walker (1960b; fig. 3) is underlain by a zone characterized by heulandite + stilbite with occasional mordenite and epistilbite. The lower zone is similar to zones characterized by heulandite and/or stilbite identified in Icelandic geothermal systems (Kristmannsdóttir and Tómasson, 1978), East Greenland (Neuhoff and others, 1997), the Faeroe Islands (Jørgensen, 1984), the North Shore Volcanic Group (Minnesota, USA; Schmidt, 1990), and the Reydarfjördur drillhole (Mehegan, Robinson, and Delaney, 1982).

Mesolite + scolecite zone alteration at Teigarhorn is characterized by radiating bundles of near stoichiometric scolecite fibers (table 3) that fill nearly all pore spaces remaining after C/S precipitation (fig. 5D). Scolecite is white in hand specimen and often has a brownish hue in plane polarized light. Growth direction is very distinct; the bundles widen as a function of distance from the apex where nucleation first occurred at the edge of Stage II C/S pore linings.

Typical vesicle fillings in the heulandite + stilbite zone consist of intergrowths of stilbite, heulandite, and mordenite with occasional epistilbite (fig. 5B, C). Frequently only one or two of these minerals are present in a given pore (usually stilbite or heulandite). Mordenite is fibrous, occurring alone or as discrete fibers within heulandite or stilbite crystals (fig. 5C). Stilbite, heulandite, and epistilbite occur as euhedral blocky to lath shaped crystals. No evidence was found for heulandite + stilbite zone assemblages overprinting (replacing) mesolite + scolecite zone minerals. Representative compositions of Stage II stilbite, heulandite, and epistilbite are given in table 3 (Stage II mordenite is too fine-grained for reliable analysis). Epistilbite compositions are slightly richer in $Al^{+3}$ and $Na^{+}$ than the ideal formula ($CaAl_2Si_6O_{16} \cdot 6H_2O$). The ratio of Si to Al in Stage II heulandite and stilbite ranges from ~2.9 to ~3.4 and ~2.9 to ~3.5, respectively. Exchangeable cation sites in Stage II heulandite (fig. 8) and stilbite (fig. 9)

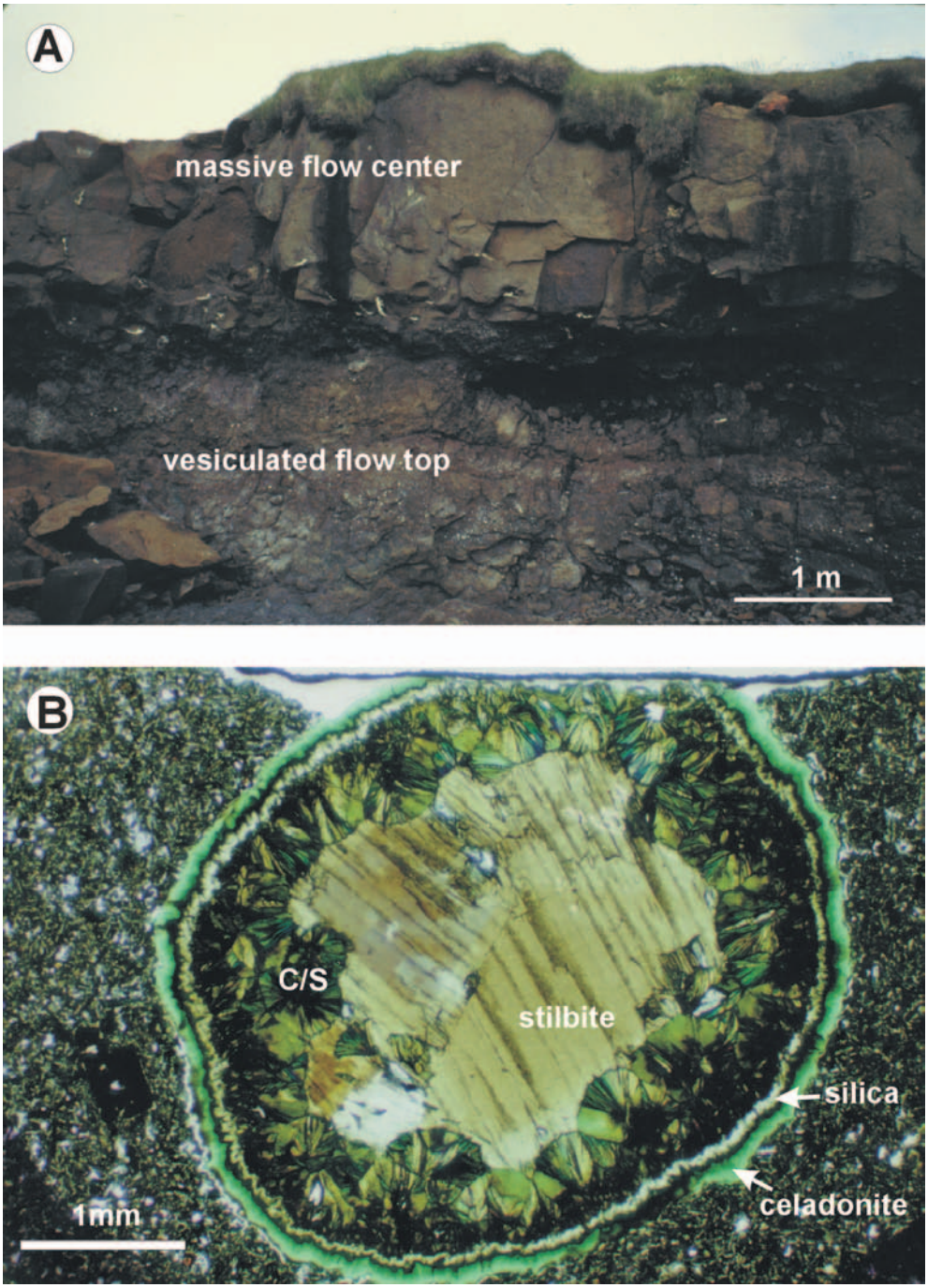


Fig. 5. Stage I and II alteration at Teigarhorn. (A) Outcrop view showing the flow scale distribution of primary pore spaces that host Stage I and II alteration. Two lava flows are visible separated by an undulating surface. The top of the lower flow is highly vesicular and contains abundant Stage I celadonite rims and Stage II scolecite visible as white pore fillings. The massive flow center of the upper flow contains only isolated, large vesicles filled with Stage II scolecite. (B) Stage I celadonite and silica rims preceding Stage II mixed-layer chlorite/smectite (C/S) and stilbite in sample ISMP-2. Photomicrograph taken with polars partially crossed. Analyses in columns 2 and 7 of table 2 were conducted on celadonite and C/S rims shown in photo.

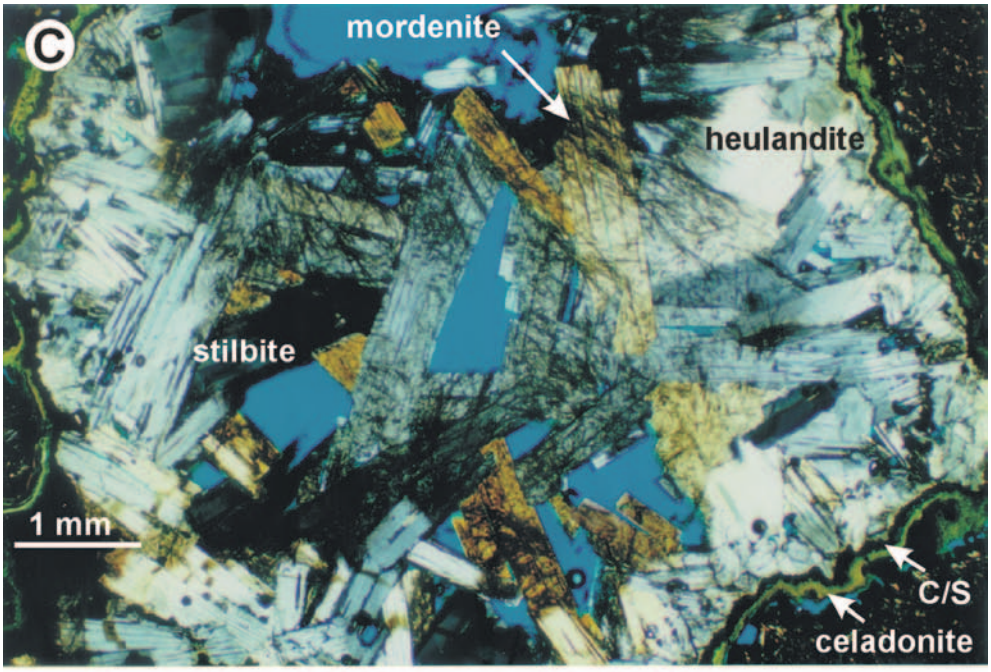


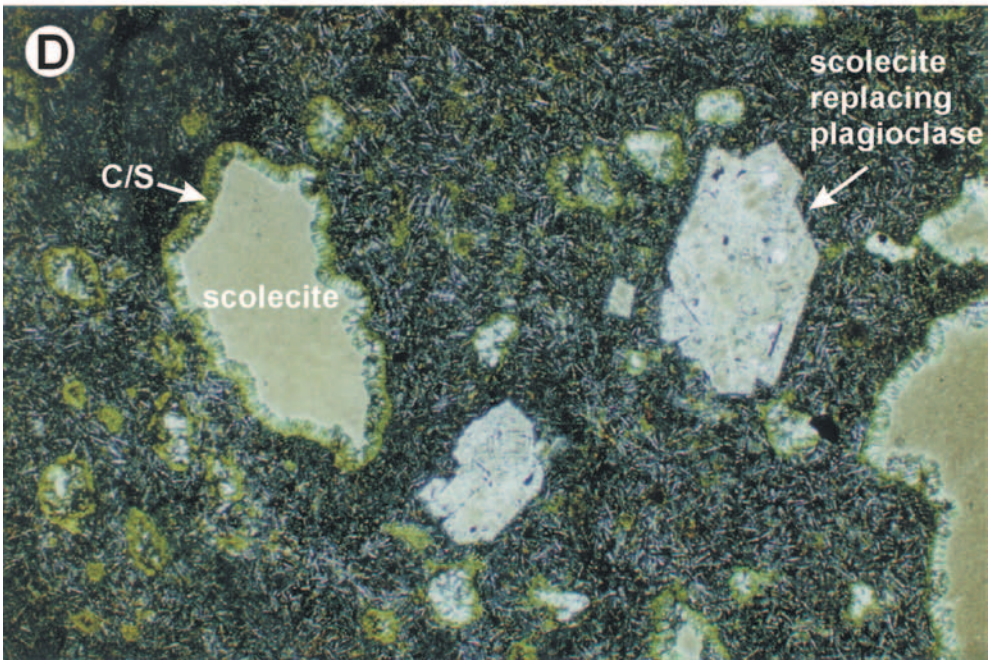


(C) Stage II heulandite + stilbite zone assemblages (sample 94-53). Photomicrograph taken with polars partially crossed. Vesicle in rimmed with celadonite (Stage I) and Stage II C/S. Filling the pore are lath-shaped crystals of stilbite (birefringement phase) and blocky crystals of heulandite. The stilbite and heulandite crystals contain abundant mordenite fibers. Blue areas are residual porosity (color due to impregnated epoxy). (D) Stage II mesolite + scolecite zone assemblages (sample 94-77). Photomicrographs taken with polars partially crossed. Vesicles are rimmed with C/S and filled with scolecite. The large plagioclase phenocrysts have been replaced by scolecite.

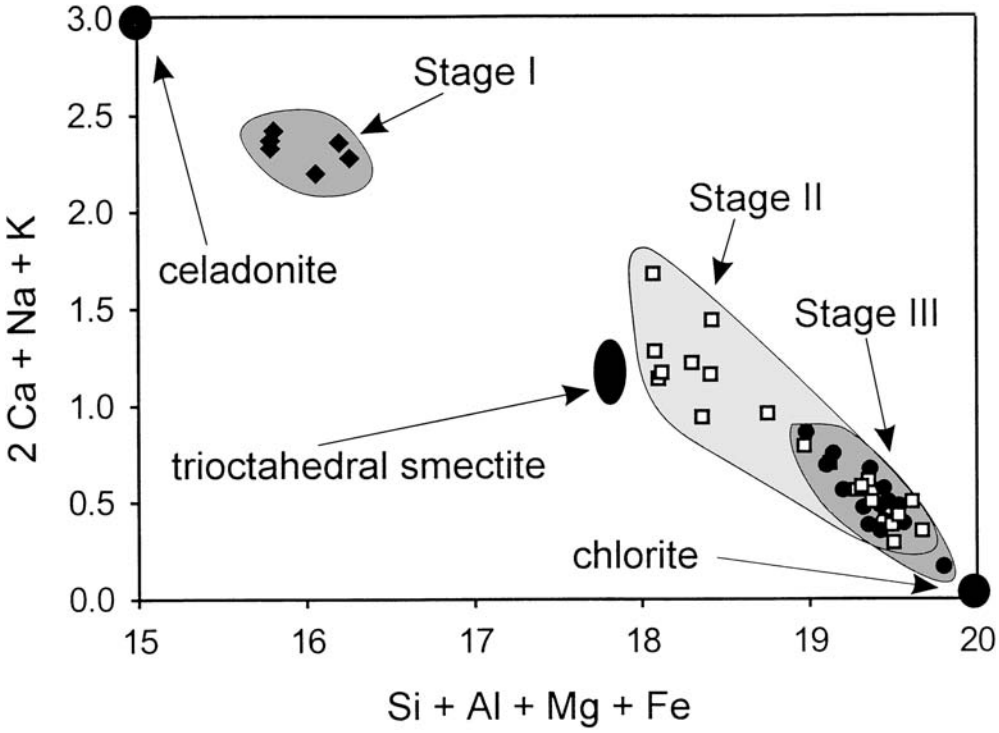


Fig. 6. Chemistry of phyllosilicates from Teigarhorn (normalized to 28 O charge equivalents) as a function of total mols of charge associated with exchangeable ions (2Ca + Na + K) and total molar Si + Al + Mg + Fe content. Stage I phyllosilicates are shown as solid diamonds, Stage II phyllosilicates as open squares, and Stage III phyllosilicates as solid circles. Ideal, endmember celadonite, chlorite, and trioctahedral smectite are plotted as large black ovals. Note restricted composition ranges for Stage I and III phyllosilicates and higher smectite contents of Stage II phyllosilicates.

are dominantly occupied by $Ca^{+2}$, although in some samples $Na^{+}$ and $K^{+}$ constitute up to 30 percent of the exchangeable ions.

Stage II minerals in the matrix of the lavas occur predominantly as pseudomorphic replacements of primary phenocryst and groundmass phases (table 1). Groundmass glass, pyroxene, and olivine as well as pyroxene and olivine phenocrysts are partially replaced by C/S with compositions similar to that lining primary pore space. Groundmass and phenocryst plagioclase is pseudomorphically replaced by scolecite and/or completely albitized (table 4).

*Stage III.*–The latest alteration at Teigarhorn (Stage III) is developed in secondary pore space (fractures, breccias, et cetera) and primary pores intersected by this porosity (figs. 10, 11). Stage I and II minerals filling vesicles and other primary pore spaces are cross cut by Stage III porosity. Stage III breccias commonly entrain Stage I and II minerals (fig. 11C). This is frequently visible in outcrop as rafts of vesicle walls coated with celadonite and Stage II heulandite within Stage III breccias. Development of fracture porosity during Stage III is associated with intrusion of mafic dikes that cross cut the lavas. The near-vertical dikes make up more than 8 percent of the volume of rocks at Teigarhorn (fig. 2) and vary in thickness between 0.5 and 3 m. Spacing between dikes is uneven, ranging from less than 1 to over 30 m. Lava flows within a few meters of the dikes are extensively fractured, but the fractures generally do not contain secondary

TABLE 2

*Representative phyllosilicate analysis from Teigarhorn, eastern Iceland determined by EPMA*

| Sample | ISMP2 celadonite | 94-53 C/S | 94-53 C/S | 94-92 C/S | 94-92 C/S | ISMP2 C/S | 94-50 C/S | 94-94 C/S |
|---|---|---|---|---|---|---|---|---|
| Stage | I | II | II | II | II | II | III | III |
| Occurrence | vesicle | vesicle | vesicle | vesicle | vesicle | vesicle | vein | vein |
| $SiO_2$ | 45.55 | 29.96 | 32.51 | 30.65 | 34.25 | 31.23 | 31.29 | 28.58 |
| $Al_2O_3$ | 6.70 | 13.49 | 12.19 | 12.27 | 9.83 | 13.59 | 11.67 | 13.58 |
| FeO | 14.06 | 30.62 | 28.64 | 31.03 | 24.09 | 27.86 | 31.90 | 33.81 |
| MnO | 0.00 | 0.35 | 0.28 | 0.00 | 0.00 | 0.42 | 0.14 | 0.30 |
| MgO | 3.83 | 11.52 | 10.83 | 10.41 | 10.68 | 13.71 | 10.97 | 11.02 |
| BaO | 0.00 | 0.00 | 0.00 | 0.00 | 0.00 | 0.00 | 0.00 | 0.00 |
| SrO | 0.00 | 0.00 | 0.00 | 0.00 | 0.00 | 0.00 | 0.00 | 0.00 |
| CaO | 0.19 | 0.56 | 0.55 | 1.01 | 1.85 | 0.79 | 0.50 | 0.32 |
| $Na_2O$ | 0.11 | 0.12 | 0.31 | 0.19 | 0.20 | 0.06 | 0.18 | 0.00 |
| $K_2O$ | 7.89 | 0.24 | 1.45 | 0.00 | 0.64 | 0.05 | 0.14 | 0.20 |
| total | 78.32 | 86.86 | 86.77 | 85.54 | 81.54 | 87.71 | 86.78 | 87.80 |
| | | | | Formula unit composition | | | | |
| Si | 7.97 | 6.57 | 7.08 | 7.05 | 7.71 | 6.65 | 6.90 | 6.33 |
| $Al^{iv}$ | 0.03 | 1.43 | 0.92 | 0.95 | 0.29 | 1.35 | 1.10 | 1.67 |
| $Al^{vi}$ | 1.35 | 2.06 | 2.20 | 2.01 | 2.31 | 2.06 | 1.92 | 1.87 |
| $Fe^{+2}$ | 2.06[2] | 5.61 | 5.21 | 5.70 | 4.53 | 4.96 | 5.87 | 6.25 |
| Mn | 0.00 | 0.06 | 0.05 | 0.00 | 0.00 | 0.08 | 0.03 | 0.06 |
| Mg | 1.00 | 3.76 | 3.51 | 3.41 | 3.58 | 4.35 | 3.60 | 3.63 |
| Ba | 0.00 | 0.00 | 0.00 | 0.00 | 0.00 | 0.00 | 0.00 | 0.00 |
| Sr | 0.00 | 0.00 | 0.00 | 0.00 | 0.00 | 0.00 | 0.00 | 0.00 |
| Ca | 0.04 | 0.13 | 0.13 | 0.31 | 0.44 | 0.18 | 0.12 | 0.08 |
| Na | 0.04 | 0.05 | 0.13 | 0.07 | 0.09 | 0.03 | 0.08 | 0.00 |
| K | 1.76 | 0.07 | 0.40 | 0.00 | 0.18 | 0.01 | 0.04 | 0.06 |
| O[1] | 22 | 28 | 28 | 28 | 28 | 28 | 28 | 28 |
| percent Chlorite | | 77.2 | 52.7 | 59.9 | 27.3 | 74.5 | 73.2 | 90.9 |

[1]oxygen charge equivalents per formula unit
[2]all iron assumed to be $Fe^{+2}$

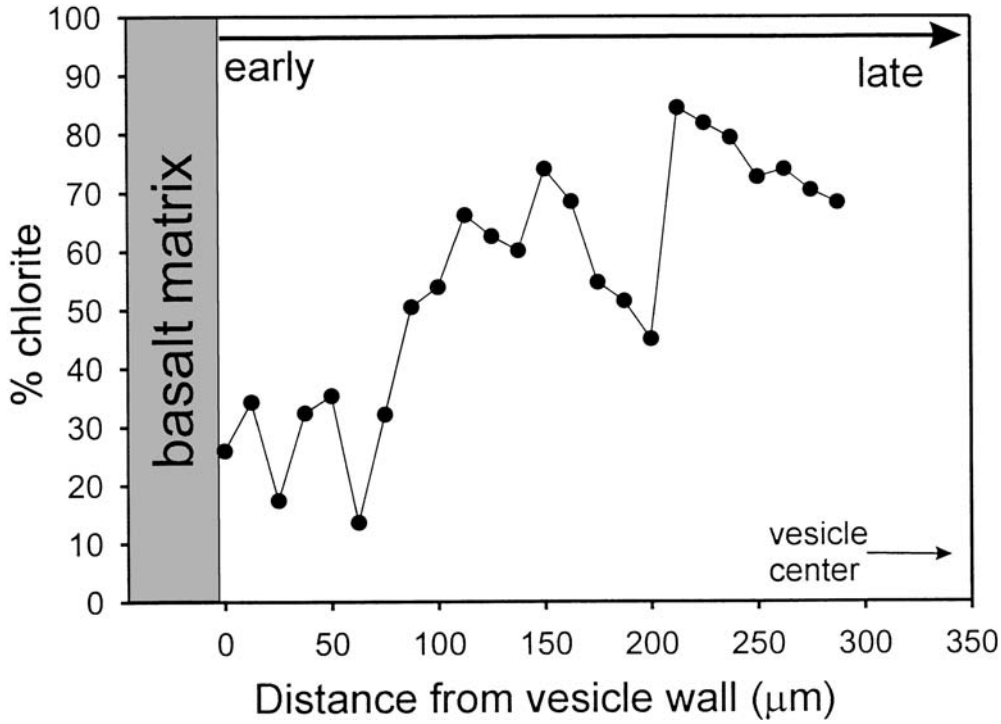


Fig. 7. Temporal changes in the compositions of Stage II mixed-layer chlorite-smectite (C/S) depicted as a function of percent chlorite (calculated using method of Schiffman and Fridleifsson, 1991). Analyses are from a 300 μm linear traverse through a Stage II clay rim of a vesicle in sample 94-50. The compositions of C/S trend from early smectitic clays (near the vesicle wall) to relatively late chloritic clays (towards the center of the vesicle).

minerals. At distances greater than 3 m from some dikes, brittle deformation features host Stage III mineral assemblages. This alteration is only locally developed.

Stage III mineral assemblages fill 0.2 to 2 cm thick veins oriented parallel to the dikes and irregular fractures and breccias up to 0.8 m across. Veins and fractures can be traced for up to 10 m. The margins of veins are occasionally lined with 5 micron equant crystals of clinoptilolite (compositions given in fig. 8 and table 5) and usually marked by one or more layers of chalcedony. Filling the veins is quartz that is an- to subhedral near the margin and euhedral in the center with the c axis oriented normal to the vein walls. Clusters of euhedral quartz crystals (individual crystal size two to four mm) frequently form stalactiform deposits hanging vertically from the roofs of large cavities in the breccias. Generally chlorite-rich C/S occurs intergrown with quartz and as discrete fracture fillings (table 2). The last assemblages to fill the veins and breccias are euhedral stilbite, heulandite, or stilbite + heulandite + mordenite (fig. 11A, B) with local development of later scolecite, laumontite, and calcite in large, open cavities (fig. 11B). Stage III zeolites frequently occur as vein fillings and as large (cm-scale) euhedral crystals for which Teigarhorn is famous. Representative compositions of Stage III zeolites are given in table 5. The compositions of heulandite, stilbite, and scolecite formed during Stage III are similar to those formed during Stage II (table 5; figs. 8 and 9).

Fluid inclusion heating/freezing experiments were conducted on a 3 cm crystal of Iceland spar type calcite that formed late in Stage III along with scolecite and laumontite. Two-phase inclusions (liquid with vapor bubbles constituting ~5 percent of the inclusion

TABLE 3

*Representative compositions of Stage II zeolites from vesicles determined by EPMA*

| | scolecite 96-T-1 | scolecite 94-80 | heulandite 94-95 | heulandite 94-35 | stilbite 96-T-1 | stilbite 94-96 | epistilbite 94-93 | epistilbite 96-T-1 |
|---|---|---|---|---|---|---|---|---|
| $SiO_2$ | 45.35 | 44.41 | 60.50 | 60.06 | 61.96 | 58.94 | 60.36 | 55.83 |
| $Al_2O_3$ | 25.77 | 24.44 | 16.36 | 16.50 | 16.48 | 17.02 | 18.02 | 16.97 |
| $Fe_2O_3$ | 0.05 | 0.06 | 0.00 | 0.04 | 0.00 | 0.00 | 0.00 | 0.03 |
| MnO | 0.00 | 0.01 | 0.00 | 0.00 | 0.00 | 0.00 | 0.00 | 0.00 |
| MgO | 0.01 | 0.00 | 0.03 | 0.01 | 0.03 | 0.07 | 0.00 | 0.04 |
| BaO | 0.02 | 0.00 | 0.18 | 0.22 | 0.24 | 0.32 | 0.13 | 0.25 |
| SrO | 0.00 | 0.00 | 0.30 | 0.90 | 0.60 | 0.56 | 0.00 | 0.24 |
| CaO | 13.12 | 13.72 | 7.32 | 7.22 | 5.96 | 7.34 | 8.04 | 6.90 |
| $Na_2O$ | 1.13 | 0.04 | 0.74 | 0.60 | 1.26 | 0.84 | 1.35 | 1.00 |
| $K_2O$ | 0.00 | 0.00 | 0.92 | 0.95 | 2.01 | 1.00 | 0.07 | 1.03 |
| total | 85.45 | 82.68 | 86.33 | 86.50 | 88.53 | 86.09 | 87.98 | 82.28 |
| | | | | Anhydrous formula unit composition | | | | |
| Si | 3.00 | 3.02 | 6.84 | 6.81 | 6.87 | 6.72 | 5.94 | 5.72 |
| Al | 2.01 | 1.96 | 2.18 | 2.19 | 2.16 | 2.28 | 2.09 | 2.29 |
| Fe | 0.00 | 0.00 | 0.00 | 0.00 | 0.00 | 0.00 | 0.00 | 0.00 |
| Mn | 0.00 | 0.00 | 0.00 | 0.00 | 0.00 | 0.00 | 0.00 | 0.00 |
| Mg | 0.00 | 0.00 | 0.00 | 0.00 | 0.00 | 0.02 | 0.00 | 0.00 |
| Ba | 0.00 | 0.00 | 0.00 | 0.00 | 0.00 | 0.02 | 0.00 | 0.00 |
| Sr | 0.00 | 0.00 | 0.02 | 0.07 | 0.04 | 0.05 | 0.00 | 0.00 |
| Ca | 0.92 | 1.01 | 0.88 | 0.88 | 0.71 | 0.88 | 0.86 | 0.98 |
| Na | 0.15 | 0.01 | 0.16 | 0.14 | 0.28 | 0.19 | 0.26 | 0.27 |
| K | 0.00 | 0.00 | 0.14 | 0.14 | 0.28 | 0.14 | 0.00 | 0.00 |
| O | 10 | 10 | 18 | 18 | 18 | 18 | 16 | 16 |

volume) occur throughout the crystal. Most inclusions are up to 0.25 mm in diameter with ovoid, elongate, or triangular morphologies. Primary inclusions homogenized at 115° ± 8°C and frozen at −0.1° to 0°C.

Stage III fractures and breccias are frequently surrounded by aureoles (1-40 cm wide) of extensive $SiO_2$ metasomatism (fig. 10). These zones are lighter in color than the surrounding lavas, and in extreme cases are pale yellow. The lava is extensively replaced by fine-grained aggregates of quartz with about 5 modal percent C/S (fig. 11C and D). Stage III C/S (table 2, fig. 6) is more chloritic than in Stage II, ranging from 55 to 90 percent chlorite. Where this alteration is most intense the original texture of the lava is completely obliterated. The replaced lava is highly porous with a spongy texture (fig. 11D) and has approx 20 percent secondary porosity.

### *Bulk Rock Chemistry*

Bulk rock compositions of samples from two successive lava flows (and an intervening mafic volcanoclastic unit) from Teigarhorn (samples 94-86, 94-87, 94-90, 94-91, 94-96, and 94-101; fig. 2) are given in table 6. Samples 94-86 and 94-101 are from the overlying (younger) flow, 94-87 is the mafic volcanoclastic horizon, and 94-90, 94-91, and 94-96 are from the underlying (older) flow (see footnote to table 6 for sample descriptions). The least altered samples of both flows (94-86 and 94-90) are similar in composition and belong to the low MgO tholeiite lavas described by Flower and others (1982). The mafic volcanoclastic unit is compositionally similar to the unaltered lavas except for higher Fe, Si, K, Rb, Cu, Cr, and Ni and lower Ca, Na, P, Sr, and V contents in the oxide-rich, more oxidized volcanoclastic horizon.

The effects of alteration on bulk rock composition can be assessed by comparing these relatively unaltered samples with examples of Stages I and II (94-91 and 94-96) and Stage III (94-101) alteration from the same flows. This is illustrated by the isocon plots

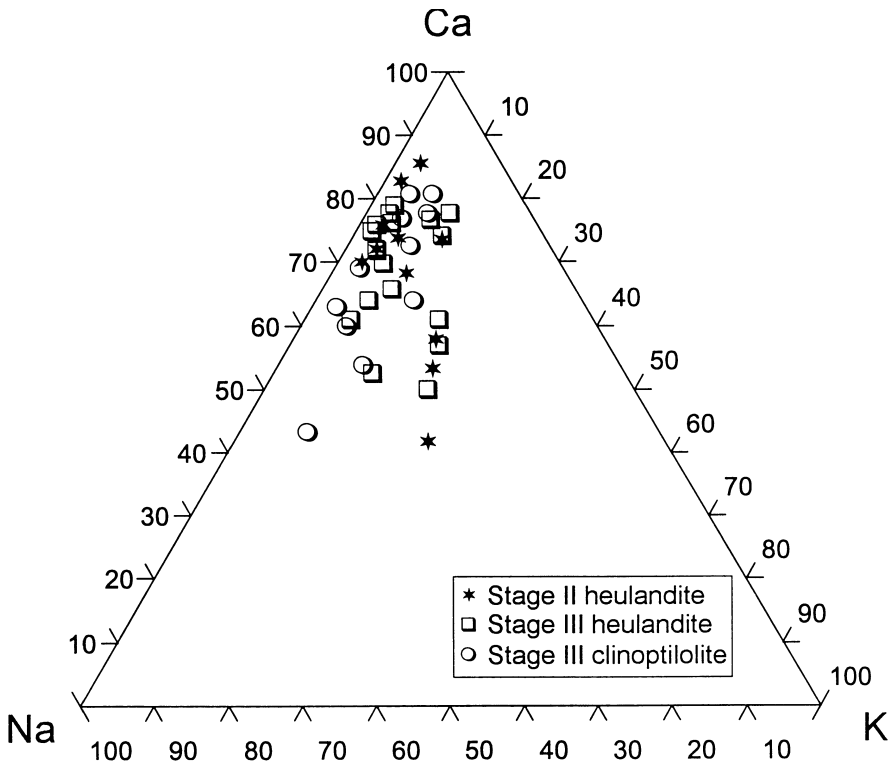


Fig. 8. Molar proportions of Ca, Na, and K in heulandite and clinoptilolite from Teigarhorn.

(Grant, 1982) in figure 12, which compare the compositions of sample 94-96 (which exhibits Stage I and II alteration) and sample 94-101 (extreme Stage III $SiO_2$ metasomatism) to those of the relatively unaltered samples 94-90 and 94-86, respectively, of the same flows. The linear trends (labeled "constant mass isocon" in fig. 12) represent no elemental loss or gain during alteration. It can be seen in figure 12A that Stage I and II alteration together lead to only minor changes in bulk rock composition, as illustrated by the fact that the major element data plot along the isocon. With the exception of Rb and La in sample 94-96, the other trace element data listed in table 6 have been omitted for clarity, but they all plot along the constant mass trend as well. The most significant bulk chemical signature of Stages I and II is an increase in La, Rb, and to a lesser extent $K_2O$ concentration; Rb and $K_2O$ were likely concentrated due to precipitation of celadonite in 94-96. The fact that most of the data in figure 12A plot along the constant mass isocon reflects the isochemical nature of the hydration reactions that typify Stage I and II alteration. In contrast, the extreme metasomatism associated with Stage III is clearly reflected in sample 94-101. Quartz along with minor stilbite and chlorite have entirely replaced the lava (94-86) resulting in a bulk rock composition that is ~92 percent $SiO_2$. As can be seen in figure 12B, this sample is clearly enriched in $SiO_2$ and depleted in all other analyzed elements relative to the unaltered lavas.

### *Porosity*

Lava flows at Teigarhorn exhibit values of $\Phi_1^*$ (volume percent of primary pores) up to 22 percent with subsequent processes during Stage III leading to values of $\Phi_2^*$ of up to 11 percent (table 7). The range of values of $\Phi_1^*$ given in table 7 is typical of basaltic lavas

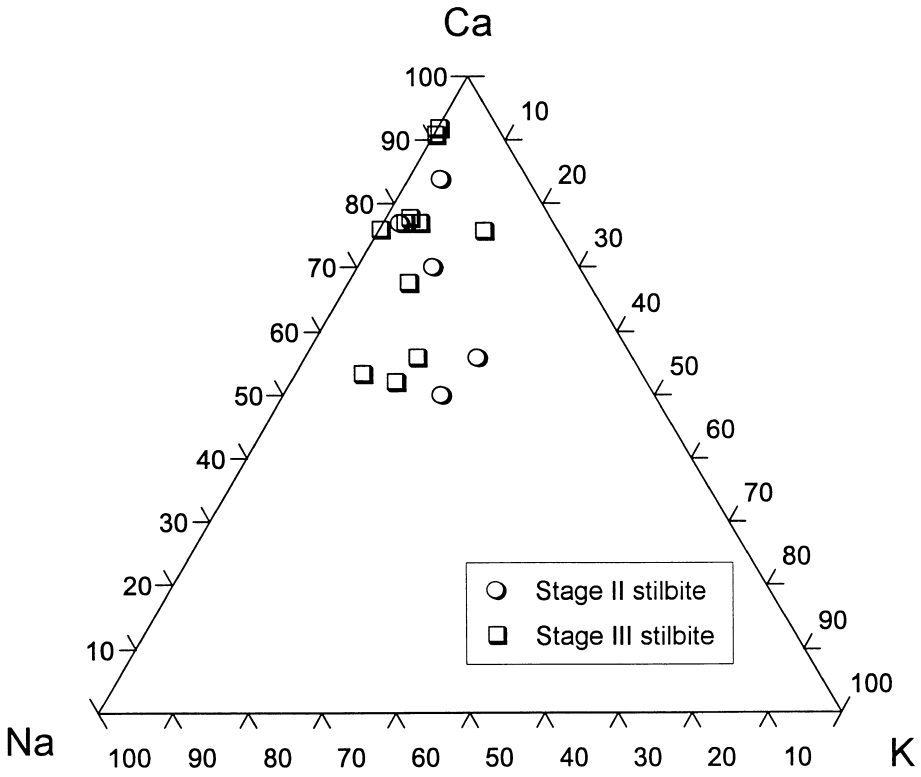


Fig. 9. Molar proportions of Ca, Na, and K in stilbite from Teigarhorn.

reported by Christensen and Wilkens (1982) from the Reydarfjördur drillhole in eastern Iceland. Variations in $\Phi_1^*$ (table 7) reflect differences in pore density both between flows and within various portions of a given flow. The estimates of $\Phi_2^*$ (volume percent of secondary pores) are similar to those obtained by Manning and Bird (1991) for fractured basalts near the margin of the Skaergaard intrusion in East Greenland.

Percentages of $\Phi_1^*$ occupied by Stage I celadonite and silica and Stage II clays and zeolites along with the percent of $\Phi_1^*$ remaining after precipitation of Stage I and II minerals are given in table 8. Inspection of the table shows that the extent of porosity reduction during surficial alteration and burial metamorphism is heterogeneous between samples and is a strong function of paragenetic stage. Precipitation of Stage I minerals, where developed, leads to a 10 to 30 percent reduction in $\Phi_1^*$. Chlorite/smectite interlayer clays are more common than Stage I minerals and fill 0 to 80 percent of $\Phi_1^*$. Zeolites, the last minerals to precipitate during Stage II, fill an additional 0 to 90 percent of $\Phi_1^*$. The percent of $\Phi_1^*$ remaining after Stage II varies between ~0 and 35 percent; that is, $\Phi$ after Stage II ranges from about 0 percent to nearly 8 percent.

## DISCUSSION

*Time-space development of mineral parageneses.*–Mineral parageneses developed at Teigarhorn present a time-integrated view of the petrogenesis of zeolite-facies basaltic aquifers in eastern Iceland. In this context, the temporal development of mineral assemblages can be directly related to the geologic evolution of the crust in eastern Iceland. This is summarized in figure 13, which depicts the history of the lavas at

TABLE 4

*Representative compositions of altered and fresh plagioclase determined by EPMA*

| | fresh plagioclase 94-91 | albitized plagioclase 94-79 | albitized plagioclase 96-T-1 |
|---|---|---|---|
| $SiO_2$ | 50.51 | 66.60 | 67.80 |
| $Al_2O_3$ | 30.37 | 19.60 | 19.47 |
| $Fe_2O_3$ | 0.80 | 0.29 | 0.05 |
| MnO | 0.00 | 0.04 | 0.00 |
| MgO | 0.16 | 0.09 | 0.02 |
| BaO | 0.04 | 0.00 | 0.04 |
| SrO | 0.08 | 0.00 | 0.04 |
| CaO | 13.43 | 0.28 | 0.51 |
| $Na_2O$ | 3.72 | 11.40 | 11.44 |
| $K_2O$ | 0.07 | 0.10 | 0.07 |
| total | 99.19 | 98.40 | 99.44 |
| | Atoms per formula unit (8 O) | | |
| Si | 2.33 | 2.97 | 2.99 |
| Al | 1.66 | 1.03 | 1.01 |
| Fe | 0.01 | 0.01 | 0.00 |
| Mn | 0.00 | 0.00 | 0.00 |
| Mg | 0.03 | 0.01 | 0.00 |
| Ba | 0.00 | 0.00 | 0.00 |
| Sr | 0.00 | 0.00 | 0.00 |
| Ca | 0.66 | 0.01 | 0.02 |
| Na | 0.34 | 0.99 | 0.98 |
| K | 0.01 | 0.00 | 0.00 |
| % Albite | 33.6 | 98.1 | 97.2 |
| % Anorthite | 65.9 | 1.3 | 2.4 |
| % Orthoclase | 0.5 | 0.6 | 0.4 |

Teigarhorn. The horizontal axis in figure 13 represents time after eruption and the vertical axis is crustal depth. Also illustrated in figure 13 are petrotectonic events (lava eruption, burial during crustal accretion, dike intrusion, glacial exhumation) and mineral parageneses experienced by the lavas.

Celadonite and silica rims (Stage I) formed at shallow depths (fig. 13). Stage I geopetal structures at Teigarhorn have orientations similar to the lava flows, and in other localities exhibit progressively more shallow dips between silica bands due to progressive tilting (Walker, 1974). This relationship suggests that the geopetal structures formed prior to tilting. Near surface genesis for Stage I minerals is consistent with the low temperatures ($< \sim 50°C$) at which celadonite forms in natural systems (Odin, 1988) and the supersaturation of Icelandic surface waters with respect to chalcedony (Gíslason and Eugster, 1987b; Gíslason, Arnórsson, and Ármannsson, 1996). Silica and potassium are among the most mobile elements in near-surface environments in Iceland (Gíslason, Arnórsson, and Ármannsson, 1996), providing components necessary for formation of celadonite and opal.

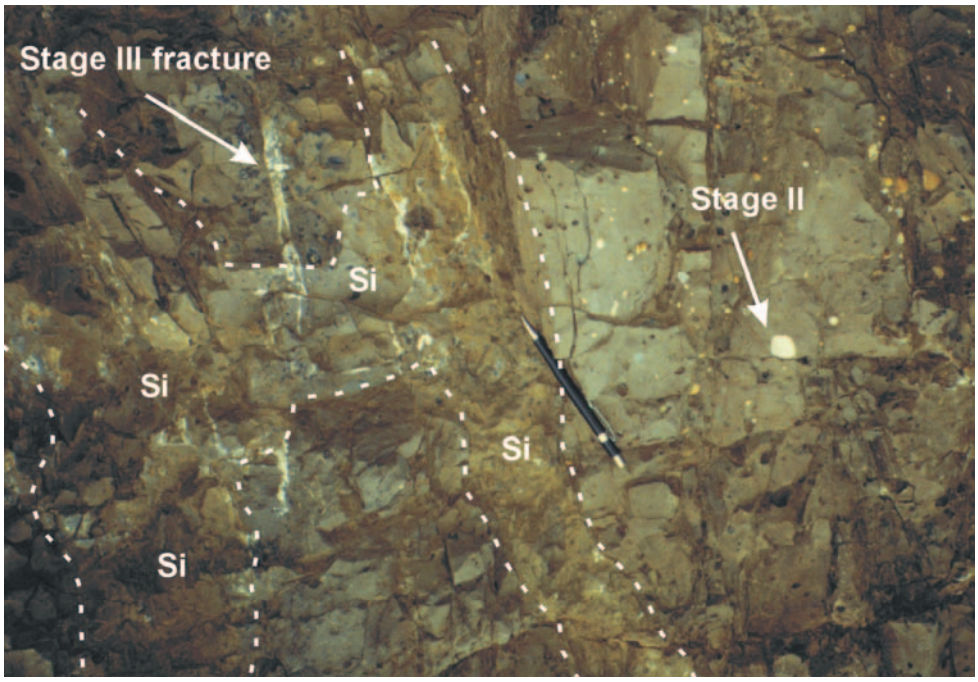


Fig. 10. Stage III fractures filled with quartz (outcrop view). Pencil for scale. The dashed white lines are boundaries of metasomatic zones containing quartz + minor C/S that replace the basalts (see fig. 11C and D). The aureoles are visible as areas of yellow alteration marked by the symbol "Si." Also visible are vesicles containing Stage II scolecite.

Burial metamorphism resulted in formation of Stage II mineral assemblages. Mixed-layer chlorite/smectite clays most likely formed during burial (fig. 13). Chemical components necessary for C/S precipitation were derived from hydrolysis of olivine and basaltic glass. We propose that the increase in chlorite content of C/S pore linings with crystallization time (fig. 7) is a consequence of progressive growth of C/S as temperature increased during burial of the lavas. The trend toward endmember chlorite composition shown in figure 7 is analogous to prograde zones characterized by smectite, C/S, and chlorite observed with increasing temperature in active geothermal systems in Iceland (Kristmannsdóttir, 1979; Schiffman and Fridleifsson, 1991). The early, more smectite-rich C/S formed at relatively low temperatures (shallow depths) and as burial proceeded C/S became progressively more chlorite-rich as temperature increased during burial.

Precipitation of Stage II zeolites occurred after burial of the lavas. Regional mineral isograds in eastern Iceland characterized by Stage II zeolites, such as the boundary between the mesolite + scolecite zone and the heulandite + stilbite zone, transgress (crosscut) the tilted volcanic stratigraphy in eastern Iceland (Walker, 1960b). The zeolite isograds thus postdate tilting of the lava pile, as observed in the Early Tertiary plateau basalts of East Greenland (Neuhoff and others, 1997). In East Greenland, the sequence of regional zeolite mineral zones with depth did not develop successively as the lavas were buried. Instead, it appears that regional zeolite formation occurred after the main stage of Early Tertiary volcanism in East Greenland ceased. The notable lack of scolecite precursors to heulandite + stilbite zone mineral assemblages at Teigarhorn suggest a similar model for the timing of zeolite zone development in eastern Iceland. Zeolites did not precipitate during burial of the lavas. The pervasive albitization observed at

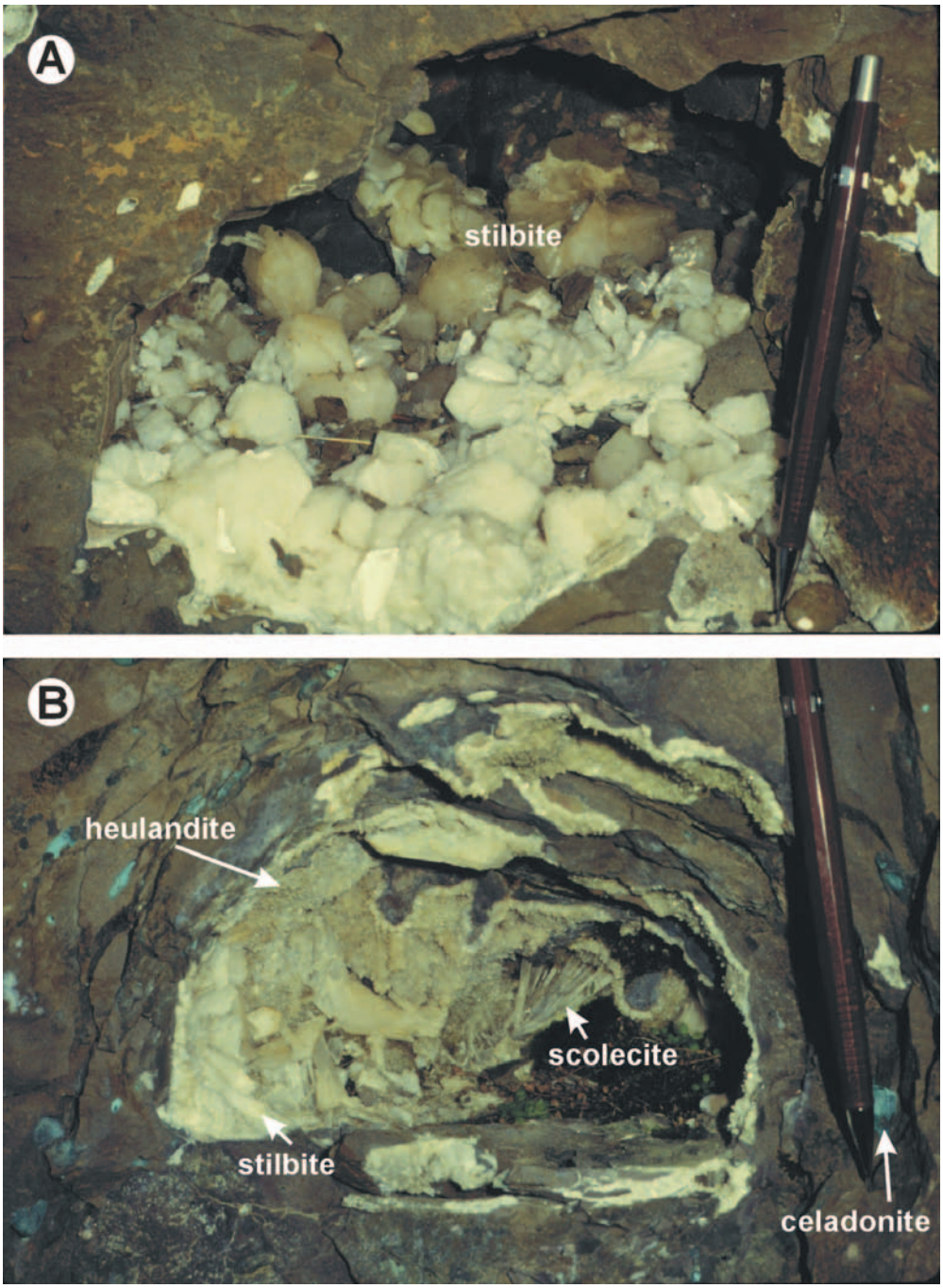


Fig. 11. Texture and mineralogy of Stage III alteration at Teigarhorn. (A) Cavity in Stage III breccia lined with euhedral stilbite. Pencil for scale. (B) Stage III breccia lined with heulandite and later stilbite and scolecite. Primary vesicles in lava around cavity are lined with green celadonite. Pencil for scale. (C) Timing and textural relationship between Stages I and III (sample 94-94). Photo taken with polars slightly crossed. The wall of a primary pore space is lined with celadonite; Stage III stilbite fills a vein along the wall of the pore. A patchy aggregate of quartz (with minor C/S) is replacing the lava on the other side of the vein. The "pie slice"–shaped celadonite in the center of the photo has been dislodged from the wall of the pore space during Stage III brecciation. Note the vuggy texture of the quartz aggregate replacing the lava (blue areas are porosity filled with impregnated epoxy). (D) Hydrothermally altered lava (sample 94-97) that has undergone extensive $SiO_2$ metasomatism. Photo taken with polars slightly crossed. The matrix of the lava is pervasively replaced by quartz and C/S. Stilbite filled cavities appear to represent both partially replaced Stage II vesicle fillings and late Stage III veins. Abundant pore space is present between quartz grains (blue areas).

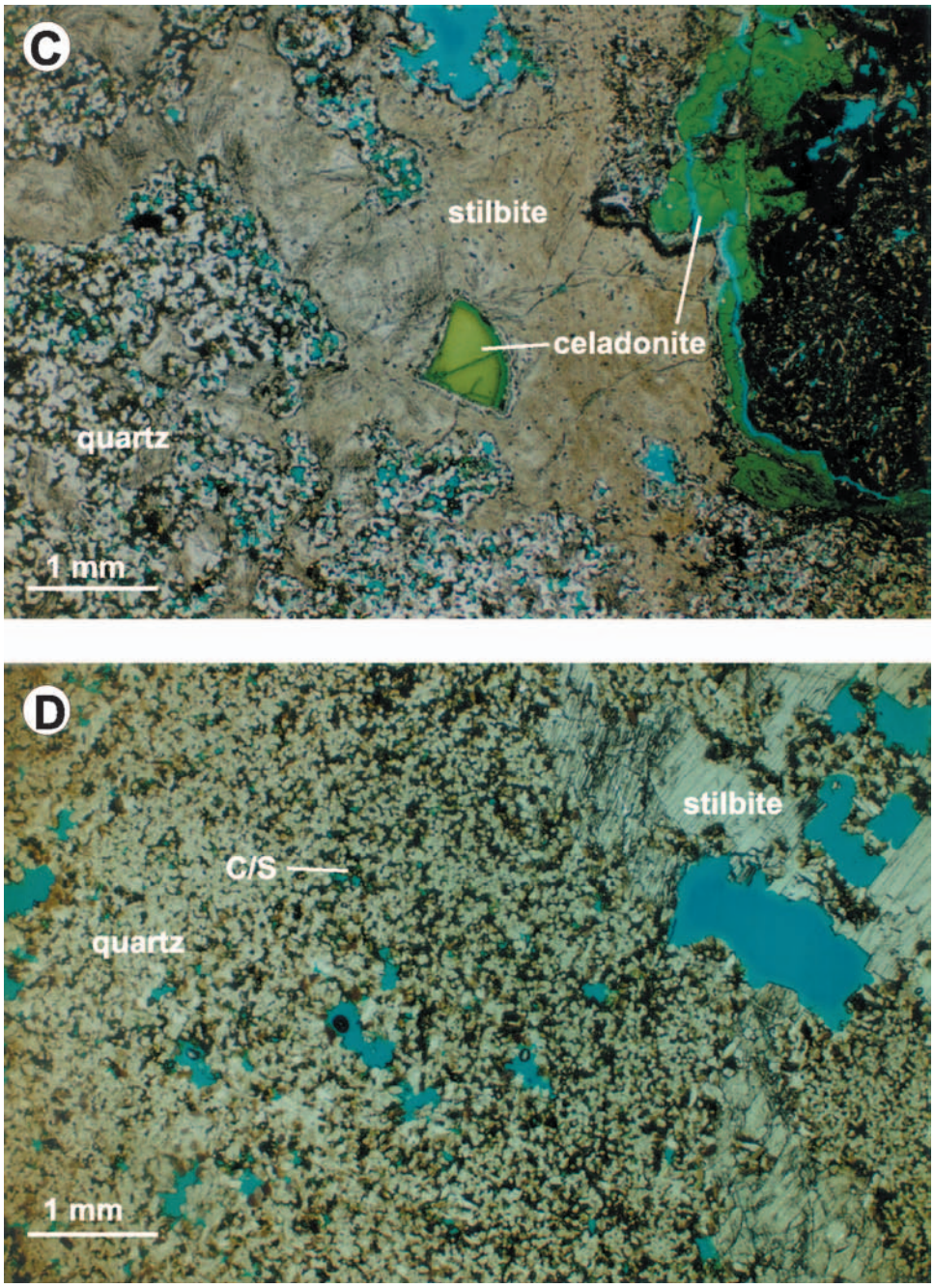


Fig. 11 (continued)

Teigarhorn is not present at elevations >100m in lavas exposed in the mountains around Berufjördur (Neuhoff, unpublished data). This suggests that albitization occurred concurrently with Stage II zeolite formation. The paucity of absolute age dates in eastern Iceland do not permit concise constraints on the timing and duration of zeolite

TABLE 5

*Representative compositions of Stage III fracture-filling zeolites determined by EPMA.*

| | clinoptilolite 94-52 | clinoptilolite 94-54 | heulandite 94-50 | mordenite 94-54 | stilbite 94-97 | stilbite ISMP2 | scolecite ISMP1 | laumontite 94-81 |
|---|---|---|---|---|---|---|---|---|
| $SiO_2$ | 67.70 | 63.901 | 59.42 | 72.67 | 58.83 | 55.75 | 46.13 | 50.58 |
| $Al_2O_3$ | 13.18 | 14.801 | 15.64 | 10.81 | 16.00 | 17.42 | 25.58 | 21.98 |
| $Fe_2O_3$ | 0.05 | 0.000 | 0.00 | 0.00 | 0.00 | 0.00 | 0.00 | 0.03 |
| MnO | 0.01 | 0.000 | 0.00 | 0.02 | 0.01 | 0.00 | 0.02 | 0.00 |
| MgO | 0.01 | 0.006 | 0.02 | 0.01 | 0.01 | 0.01 | 0.00 | 0.00 |
| BaO | 0.01 | 0.087 | 0.18 | 0.04 | 0.25 | 0.41 | 0.03 | 0.01 |
| SrO | 0.10 | 0.115 | 0.26 | 0.05 | 0.25 | 0.31 | 0.07 | 0.04 |
| CaO | 5.67 | 7.007 | 6.63 | 4.25 | 7.51 | 7.72 | 13.87 | 11.32 |
| $Na_2O$ | 0.69 | 0.713 | 1.37 | 1.35 | 0.66 | 1.19 | 0.13 | 0.27 |
| $K_2O$ | 0.51 | 0.342 | 0.77 | 0.32 | 0.75 | 0.26 | 0.00 | 0.18 |
| total | 87.95 | 86.97 | 84.29 | 89.52 | 84.27 | 83.07 | 85.82 | 84.39 |
| | | | | Anhydrous formula unit composition | | | | |
| Si | 14.72 | 14.15 | 6.88 | 5.11 | 6.81 | 6.59 | 3.03 | 3.98 |
| Al | 3.46 | 3.89 | 2.13 | 0.90 | 2.19 | 2.42 | 1.98 | 2.04 |
| Fe | 0.00 | 0.00 | 0.00 | 0.00 | 0.00 | 0.00 | 0.00 | 0.00 |
| Mn | 0.00 | 0.00 | 0.00 | 0.00 | 0.00 | 0.00 | 0.00 | 0.00 |
| Mg | 0.00 | 0.00 | 0.00 | 0.00 | 0.00 | 0.00 | 0.00 | 0.00 |
| Ba | 0.00 | 0.00 | 0.00 | 0.00 | 0.00 | 0.02 | 0.00 | 0.00 |
| Sr | 0.00 | 0.00 | 0.02 | 0.00 | 0.02 | 0.02 | 0.00 | 0.00 |
| Ca | 1.30 | 1.66 | 0.82 | 0.49 | 0.94 | 0.99 | 0.97 | 0.95 |
| Na | 0.32 | 0.32 | 0.31 | 0.09 | 0.14 | 0.27 | .001 | 0.05 |
| K | 0.14 | 0.11 | 0.11 | 0.06 | 0.12 | 0.05 | 0.00 | 0.02 |
| O | 36 | 36 | 18 | 12 | 18 | 18 | 10 | 12 |

TABLE 6

*Bulk rock compositions from Teigarhorn, eastern Iceland*

| Samples‡ | 94-86 | 94-87 | 94-90 | 94-91 | 94-96 | 94-101 |
|---|---|---|---|---|---|---|
| $SiO_2$* | 46.844 | 48.145 | 46.021 | 47.414 | 47.058 | 92.210 |
| $TiO_2$* | 3.710 | 3.642 | 3.457 | 3.379 | 3.396 | 0.326 |
| $Al_2O_3$* | 13.533 | 13.068 | 13.895 | 13.531 | 13.305 | 2.558 |
| $Fe_2O_3$*,† | 17.004 | 20.301 | 17.077 | 16.632 | 16.616 | 2.574 |
| MnO* | 0.329 | 0.140 | 0.253 | 0.234 | 0.251 | 0.024 |
| MgO* | 5.212 | 5.746 | 5.750 | 5.520 | 5.399 | 0.939 |
| CaO* | 9.261 | 5.738 | 9.991 | 10.076 | 9.676 | 0.987 |
| $Na_2O$* | 3.163 | 1.812 | 2.946 | 2.868 | 3.113 | 0.551 |
| $K_2O$* | 0.763 | 1.633 | 0.322 | 0.280 | 0.519 | 0.236 |
| $P_2O_5$* | 0.442 | 0.289 | 0.398 | 0.382 | 0.387 | 0.043 |
| Total* | 100.261 | 100.514 | 100.110 | 100.316 | 99.720 | 100.448 |
| | | | | | | |
| $H_2O^-$§ | 1.372 | 6.257 | 1.955 | 2.092 | 1.029 | 0.755 |
| $H_2O^+$§ | 0.134 | 3.169 | 0.483 | 0.605 | 0.527 | 1.640 |
| | | | | | | |
| Nb† | 24.5 | 20.3 | 23.2 | 22.4 | 22.6 | 2.6 |
| Zr† | 238 | 208.3 | 217.9 | 210.3 | 212.7 | 26.1 |
| Y† | 47.2 | 39.3 | 42.6 | 41 | 42.5 | 3.8 |
| Sr† | 291 | 111.8 | 301.9 | 305.2 | 283.9 | 205.8 |
| U† | 1.6 | 0.8 | 1.4 | 1.3 | 2.2 | 0.9 |
| Rb† | 17.1 | 56.9 | 0.9 | 1.2 | 15.9 | 2.6 |
| Th† | 4.1 | 1.2 | 0.2 | 3.6 | 3.3 | B/D |
| Pb† | 2.7 | 2 | 2.8 | 0.4 | 3.5 | 0.1 |
| Ga† | 28 | 23.7 | 25.1 | 23.4 | 24 | 6.1 |
| Zn† | 148.6 | 163.1 | 143.4 | 134.5 | 128.4 | 22.6 |
| Cu† | 173.6 | 241.9 | 154.7 | 104.1 | 134.9 | 39 |
| Ni† | 29.6 | 52.4 | 38.7 | 39.5 | 37.4 | 5.9 |
| Cr† | 6 | 55.4 | 33.2 | 38.3 | 29.6 | 2.8 |
| V† | 434.6 | 354 | 454.4 | 439.4 | 428 | 46.4 |
| Ce† | 47 | 24.1 | 31.7 | 30.9 | 6.3 | 19 |
| Ba† | 180.1 | 111.7 | 120.2 | 126.7 | 103.3 | 107.7 |
| La† | 24.3 | 14.8 | 16.1 | 27.2 | 21.3 | B/D |

‡Sample descriptions:
94-86: compact lava with minor Stage III heulandite veins
94-87: bright red mafic volcanoclastic unit marking boundary between two lava flows
94-90: compact, massive lava with minor small vesicles filled with smectite
94-91: compact basalt with minor vesicles containing Stage II clay minerals
94-96: vesicular lava with abundant Stage I celadonite, Stage II heulandite and smectite
94-101: yellow, $SiO_2$-metasomatized lava from aureole around Stage III breccia
*Weight percent of oxide in anhydrous (calcined) sample. †Total Fe reported as Fe203. §Determined by loss on ignition at 110°C ($H_2O^-$) and 900°C ($H_2O^+$). †Parts per million of element in untreated sample. B/D: below detection limit.

precipitation during Stage II; however, it seems likely that it did not last more than a few Ma, as observed in East Greenland (Neuhoff and others, 1997).

Pore structures filled with Stage III alteration cross-cut Stage II mineralization. Stage III is spatially and, presumably, temporally linked to dike intrusion (fig. 13). The spatial association of Stage III with late dikes indicates that this last paragenetic stage is a local, and not a regional, phenomenon. The close association with dike intrusion indicates that Stage III occurred while the region around Teigarhorn was still undergoing intrusive

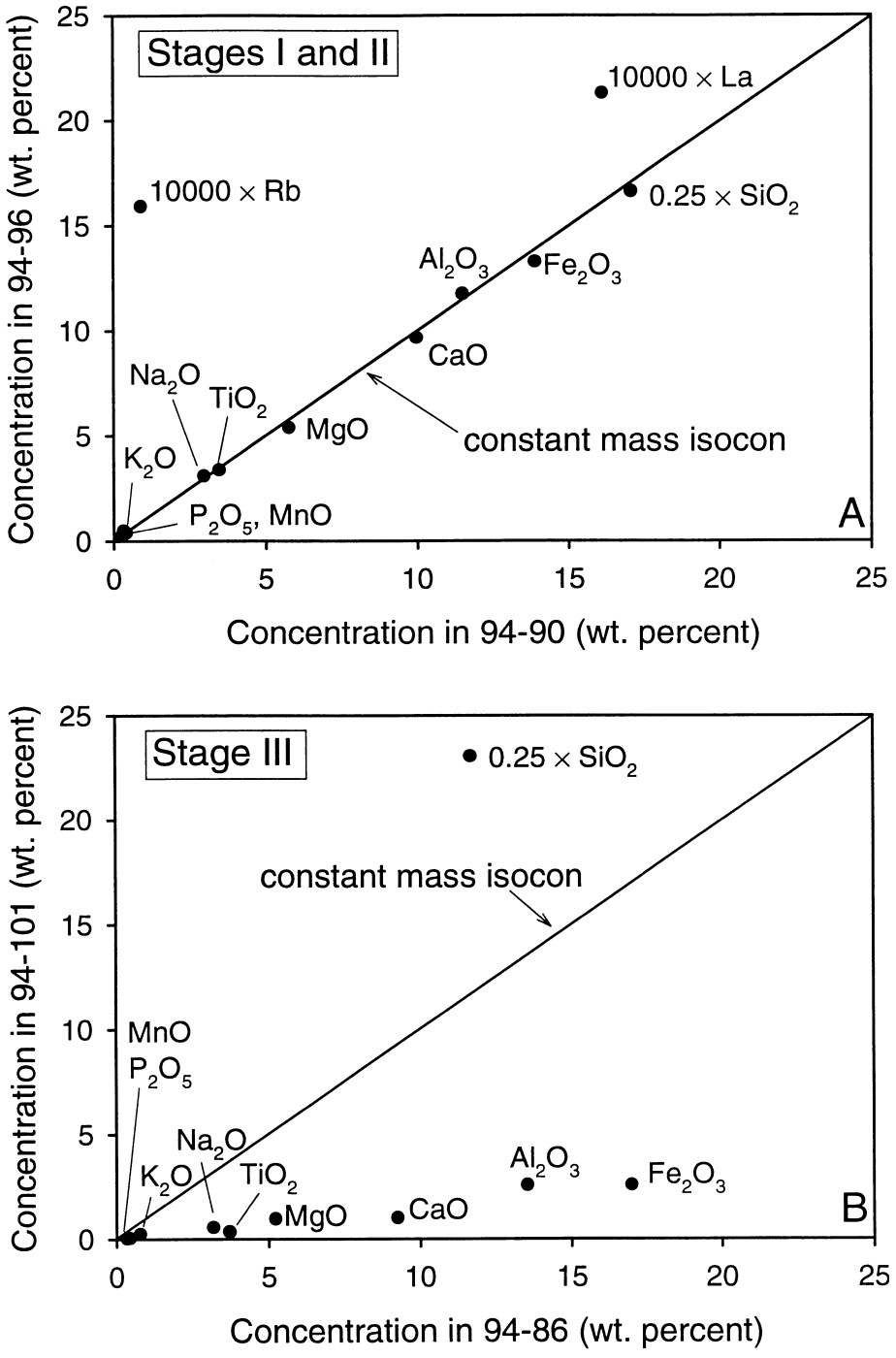


Fig. 12. Isocon plots (Grant, 1982) depicting the variation in bulk rock chemistry accompanying Stages I and II (A) and Stage III (B) alteration at Teigarhorn. The lines labeled "constant mass isocon" depict the theoretical distribution of data assuming that the mass and compositions of the lavas do not change during alteration. The $SiO_2$, Rb, and La analyses have been multiplied (by factors of 0.25, 10000, and 10000, respectively) to facilitate comparison with data for other major oxide components. Data used to construct this plot are listed in table 6.

TABLE 7

*Outcrop porosity measurements*

| Station[1] | Primary Porosity ($\Phi_1$*; %) | Secondary Porosity ($\Phi_2$*) | | |
|---|---|---|---|---|
| | | Survey Area ($cm^2$) | Pore Area ($cm^2$) | Porosity (%) |
| 1 | 22 | - | - | - |
| 2 | 4 | 60000 | 6894 | 11 |
| 3 | 12 | - | - | - |
| 4 | 4 | - | - | - |
| 5 | 6 | - | - | - |
| 6 | 17 | - | - | - |
| 7 | 4 | 56000 | 1696 | 3 |
| 8 | 12 | 34000 | 1046 | 3 |

[1]Station locations given in figure 2. Descriptions: (1) flow top; (2) flow center with abundant Stage III fractures developed ~10 m from dike; (3) flow top; (4) flow center; (5) flow center; (6) flow top; (7) flow center with abundant Stage III fractures developed ~15 m from dike; (8) flow bottom with abundant Stage III fractures developed about 5 m from dike.

TABLE 8

*Percent of pore space occupied by Stage I and II minerals based on thin section area measurement. All samples are from flow tops*

| | | Percent of Total Primary Pore Space ($\Phi_1$*) | | | | |
|---|---|---|---|---|---|---|
| **Sample** | **N[a]** | **celadonite[b]** | **silica rim[b]** | **C/S clay[c]** | **zeolites[d]** | **residual porosity[e]** |
| **94-35** | 1 | 0 | 0 | 27 | 73 | 0 |
| **94-79** | 2 | 0 | 0 | 74 | 23 | 3 |
| **94-80** | 12 | 0 | 0 | 63 | 37 | 0 |
| **94-88** | 15 | 0 | 0 | 0 | 91 | 9 |
| **94-89** | 2 | 31 | 0 | 0 | 69 | 0 |
| **94-91** | 1 | 0 | 0 | 66 | 0 | 34 |
| **94-92** | 1 | 0 | 0 | 0 | 71 | 29 |
| **94-93** | 12 | 0 | 6 | 70 | 13 | 11 |
| **94-96** | 2 | 23 | 0 | 77 | 0 | 0 |
| **ISMP2** | 1 | 13 | 5 | 48 | 35 | 0 |
| ***AVERAGE*** | **49** | **7** | **1** | **42** | **41** | **9** |

[a]Number of individual pores measured. [b]Rims of paragenetic Stage I celadonite or silica on vesicle walls. [c]Includes all paragenetic Stage II trioctahedral smectite and chlorite interlayer clays. [d]Stage II zeolite assemblages, dominantly mesolite + scolecite and heulandite + stilbite + mordenite. [e]Primary pore space ($\Phi_1^*$) remaining after paragenetic Stage II.

activity related to rifting. Increased heat flow and permeability due to fracturing during dike emplacement initiated hydrothermal fluid circulation that led to the extensive wall-rock replacement and fracture filling characteristic of Stage III mineralization. No age dating has been conducted on the dikes at Teigarhorn that would permit constraints on the absolute timing of Stage III alteration.

*Thermobarometric conditions during Stages II and III.*–Barometric conditions during paragenetic Stages II and III were complex functions of the burial and hydrogeologic

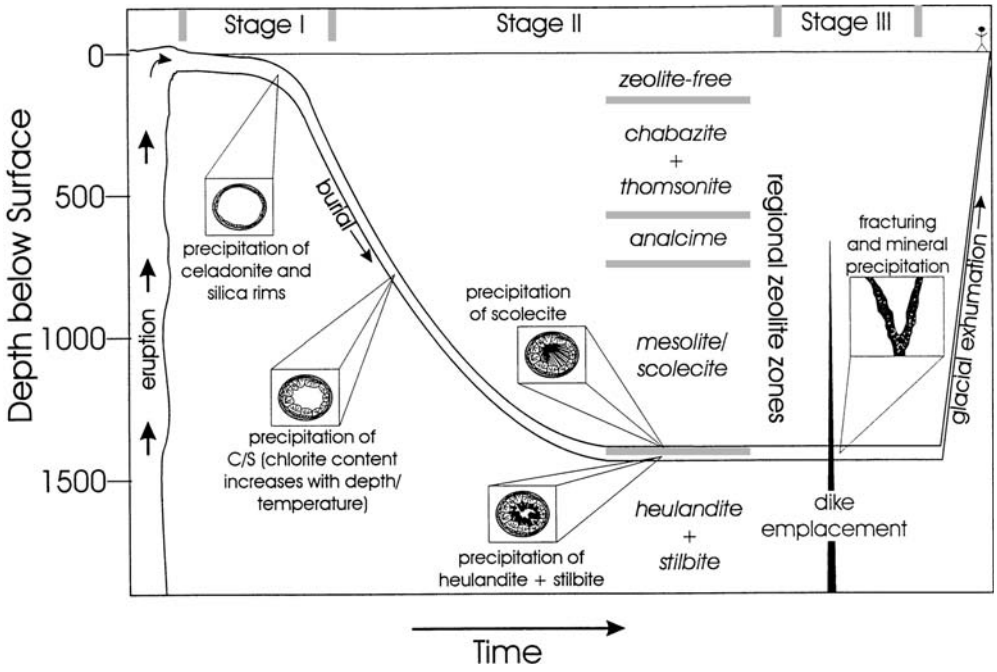


Fig. 13. Spatial and temporal development of pore-filling mineral assemblages at Teigarhorn. The vertical axis depicts depth below land surface at the time of each event depicted in the figure. Time elapsed after eruption increases to the right. No scale is implied on the horizontal axis. The parallel curves on the figure are boundaries of the lavas exposed at Teigarhorn in space and time. Note that the timing of dike emplacement is meant to infer only the timing of dikes associated with Stage III alteration at Teigarhorn.

history. Pressures during precipitation of Stage II C/S increased from a minimum of 1 bar (atmospheric pressure) to pressures between ~170 and ~500 bar, corresponding, respectively, to hydrostatic and lithostatic pressures at the maximum burial depth of 1500 m for the lavas at Teigarhorn (Walker, 1960b). Occlusion of macroscopic porosity by Stage II clay and zeolite minerals (table 8) likely resulted in near-lithostatic pressures. Pressures during Stage III were probably closer to hydrostatic conditions due to the higher permeability of continuous fractures (see below).

Although the systematic changes in Stage II C/S compositions appear to record the thermal history of the lavas (see above), the occurrence of this phase along with scolecite, stilbite, heulandite, and other Stage II zeolites is in contrast with the distribution of these minerals in active Icelandic geothermal systems. Smectite is present at low temperatures in Icelandic geothermal systems (below 200°C), with C/S occurring between 200° and 220°C (Kristmannsdóttir, 1979) and in some fields up to 270°C (Schiffman and Fridleifsson, 1991). At higher temperatures chlorite is present. Thus, C/S in Icelandic geothermal systems occurs at temperatures >100°C higher than the boundary between the mesolite + scolecite zone and stilbite zones (90° ± 10 °C; Kristmannsdóttir and Tómasson, 1978).

In regionally metamorphosed basalts, the boundary between zones characterized by smectite and C/S is generally observed under zeolite-facies conditions (Schmidt and Robinson, 1997; Robinson, Bevins, and Rowbotham, 1993; Bevins, Robinson, and Rowbotham, 1991). For example, in the North Shore volcanic group of Minnesota, smectite coexists with heulandite and stilbite; C/S is associated with higher grade laumontite-albite assemblages (Schmidt and Robinson, 1997). Based on the association of C/S with scolecite and heulandite + stilbite at Teigarhorn, C/S formed at even lower

grades during Stage II in eastern Iceland. The relatively high chlorite contents of C/S associated with the zeolite assemblages at Teigarhorn may be a consequence of albitization of primary plagioclases, which promotes chlorite formation through release of aluminum (Shau and Peacor, 1992; Schmidt and Robinson, 1997). As noted by Schiffman and Fridleifsson (1991), the temperatures at which C/S occurs in geothermal systems are often higher than in regional diagenetic systems. In contrast, temperature estimates based on zeolite assemblages and fluid inclusion thermometry are similar (see below). This suggests that estimation of temperatures from observations of zeolite assemblages in geothermal systems may be more reliable than similar estimates based on phyllosilicate distribution.

Assuming a temperature of formation for Stage II zeolite assemblages of 90° ± 10°C (see above) leads to an estimated thermal gradient of approx 53° ± 7°C/km (given a surface temperature of 10°C). A thermal conductivity for water-saturated basalt of 1.5 to 2.0 W/(mK) (Oxburgh and Agrell, 1982) gives an estimated heat flow during Stage II zeolite precipitation of 1.9 to 3.2 heat flow units (HFU = $10^{-6}$ cal · $cm^{-2}$ · $s^{-1}$). This value is consistent with conditions on the flank of the present-day active volcanic zone in Iceland (Flóvenz and Sæmundsson, 1993).

Mineral assemblages and fluid inclusion measurements indicate that temperatures during Stage III were slightly higher than in Stage II. Empirically-based chlorite geothermometry (Cathelineau, 1988; Cathelineau and Nieva, 1985) suggests that the relatively early, chlorite-rich Stage III C/S formed at temperatures between 140° and 180°C. It should be noted that temperatures estimated using chlorite geothermometry generally disagree with measured temperatures in Icelandic geothermal systems (Schiffman and Fridleifsson, 1991). Late Stage III zeolite assemblages are broadly similar to those in Stage II but may have formed at slightly higher temperatures based on the presence of laumontite. Laumontite becomes prominent at temperatures above 120°C in Icelandic geothermal systems (Kristmannsdóttir and Tómasson, 1978), consistent with pressure corrected homogenization temperatures for late-Stage III calcite (125° ± 8°C assuming hydrostatic pressures). The apparent decrease in temperature during Stage III may reflect dissipation of heat flow associated with crystallization of the dikes or may be the result of errors associated with the chlorite geothermometer noted above.

*Chemical fluxes during alteration.*–The widespread precipitation of phyllosilicates, silica minerals, and zeolites in pore spaces during Stages I and II indicates that Si, Al, Ca, Na, K, Fe, and Mg were mobile over scales of a millimeter or more. This is further illustrated by the textural preservation of pore walls and by successive lining of pore spaces during mineral paragenesis, which require that chemical components necessary for precipitation of secondary minerals were transported into the pores. All components necessary to form the mineral assemblages described above were readily available in the primary phases in the lavas (glass, olivine, plagioclase, pyroxene) with the exception of $H_2O$, which was provided by the metamorphic fluids. The similarity between the bulk rock compositions of lavas altered during Stages I and II and those of unaltered lavas (table 6; fig. 12A) indicates that many elements were relatively immobile (that is, conserved) on the scale of individual lava flows during regional alteration. An exception is potassium, which is concentrated during Stage I in celadonite (table 6). As noted above, potassium is very mobile during near-surface alteration of basaltic lavas (Gíslason, Arnórsson, and Ármannsson, 1996). The concentration of Rb, $K_2O$, and La apparent in figure 12A and table 6 is consistent with the observations of Wood (1976) that these elements were mobilized during zeolite-facies metamorphism.

In contrast, high fluid fluxes through some Stage III (see below) fractures resulted in widespread leaching at the outcrop scale of all elements except silicon (table 6; fig. 12B). Extensive replacement of the lavas by quartz (plus minor chlorite-rich C/S) is suggestive of interaction with acidic fluids. The low pH of these fluids may reflect the presence of

relatively large amounts of dissolved magmatic gases. The solubilities of primary phases in the lavas as well as C/S and zeolites are all enhanced under very acidic conditions. In contrast, quartz solubility is insensitive to pH under acidic conditions, and it formed early during Stage III from $SiO_2$ released during hydrolysis/dissolution of primary phases. The large model abundance (>90 percent) of quartz in Stage III aureoles suggests that some $SiO_2$ may have been added during alteration. Aside from minor C/S precipitated in the aureoles and later in veins, no mineralogical sinks for iron and magnesium formed during Stage III, suggesting that these elements were transported over distances of meters (the scale of outcrops at Teigarhorn) away from their sources. Late precipitation of zeolites and calcite in Stage III veins most likely occurred as the aqueous solutions became more alkaline as protons were consumed by hydrolysis.

Both Stages II and III exhibit a pronounced temporal change during paragenesis from phyllosilicates + quartz to assemblages dominated by Ca-zeolites. In both cases, this paragenetic trend was probably coincident with changes in temperature and pressure. However, the abrupt shift in the mineral composition from C/S to zeolites must reflect the chemical evolution of the aqueous electrolyte solutions from which these minerals precipitated, as schematically illustrated in the phase diagram in figure 14. The arrows A and B in figure 14 represent two possible trends in fluid composition that would result in mineral paragenesis of Ca-zeolites after C/S (figs. 4, 5B and C). The decrease in log $[(a_{Mg^{+2}}/(a_{H^+})^2]$ suggested by paragenetic trends A and B would result from decreasing the activity of $Mg^{+2}$ in the pore fluid as a consequence of precipitation of C/S (represented by clinochlore in the phase diagram). Mineralogical sources of $Mg^{+2}$ (olivine, basaltic glass) in basaltic lavas are generally less stable than plagioclase under low-grade metamorphic conditions (Gíslason and Eugster, 1987a; Gíslason and Arnórsson, 1993) and are often hydrolyzed before plagioclase. Albitization of plagioclase was likely contemporaneous with precipitation of zeolites in pores during Stage II (see above), adding $Ca^{+2}$ to aqueous solution and increasing log $([a_{Ca^{+2}})/(a_{H^+})^2]$ as suggested by trend A in figure 14. Instability of zeolites relative to C/S during early Stage II alteration provides an explanation for the apparent lack of zeolite formation during burial of the lavas inferred from our petrographic observations that heulandite + stilbite zone assemblages do not replace mesolite/scolecite zone assemblages. These observations, combined with the phase relations depicted in figure 14, suggest that the lavas were buried before olivine and basaltic glass were exhausted, resulting in fluid compositions during burial in which C/S was stable relative to zeolites.

The general paragenetic trend from C/S to zeolites, as well as fluid composition trends A and B in figure 14, is consistent with the results of experimental simulations of basalt-meteoric water interaction at low temperatures. Ghiara and others (1993) conducted experiments on closed-system dissolution of basaltic glass in deionized water at 200°C that resulted in a mineral paragenesis of early smectite + phillipsite followed by analcime. Total Mg concentrations in solution during these experiments initially rose rapidly, and then declined to a steady state level as Mg-rich smectite precipitated. Calcium concentrations also rose rapidly during the initial stages of these experiments, and continued to increase until the last stages of the experiments. Thus, log $[(a_{Ca^{+2}})/(a_{Mg^{+2}})]$ increased with time in response to precipitation of Mg-rich smectite and the fluids evolved toward the stability fields of zeolites as suggested in figure 14. Similar experiments by Gíslason and Eugster (1987a) on dissolution of basaltic glass and crystalline basalt at 25°, 45°, and 65°C resulted in nearly identical solution composition trends. Subsequent analysis of the solid phases produced in these experiments (Gíslason, Veblen, and Livi, 1993) identified several magnesium-bearing phases (kerolite, chrysotile, talc, and smectite) along with quartz, calcite, kaolinite, and amorphous precipitates. Early formation of magnesian minerals in these experiments (including smectite) con-

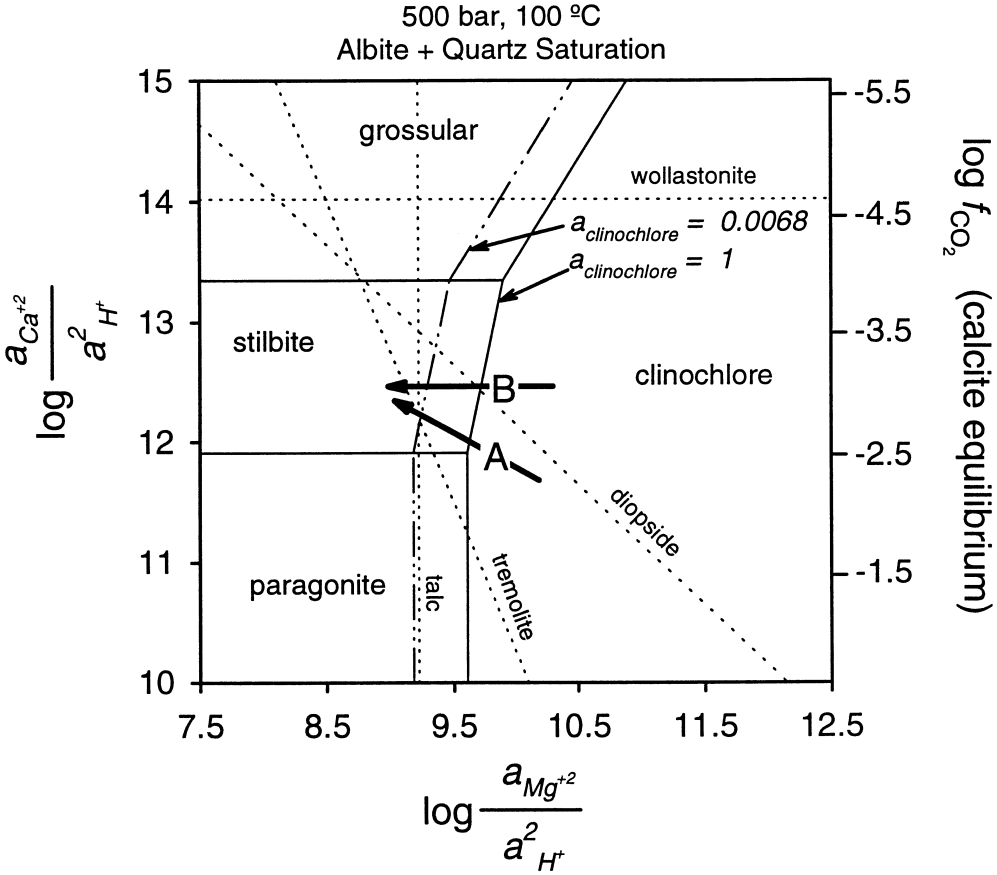


Fig. 14. Stabilities of minerals in the system MgO-CaO-$Na_2O_3$-$Al_2O_3$-$SiO_2$-$H_2O$-HCl at 100°C, 500 bar in equilibrium with quartz and albite as functions of log $[(a_{Ca^{+2}})/(a_{H^+})^2]$ and log $[(a_{Mg^{+2}})/(a_{H^+})^2]$ in an aqueous solution with $a_{H_2O}$ = 1. Diagram calculated using thermodynamic properties and algorithms in the computer code SUPCRT92 of Johnson, Oelkers, and Helgeson (1992), with addition of data for stilbite ($CaAl_2Si_7O_{18} \cdot 7H_2O$; $\Delta G^o_f$ (cal/mol) = −2381234; $\Delta H^o_f$ (cal/mol) = −25588306; $S^o$ (cal/molK) = 191.41; $V^o$ ($cm^3$/mol) = 332.61; $C^o_p$ (cal/molK) = 154.12 + 0.168 T(K) − 10860000 $T(K)^{-2}$; Neuhoff, unpublished data). The diagram was constructed for conditions approximating the maximum burial temperature and lithostatic pressure at Teigarhorn (see text). The right-hand axis gives values of log $f_{co_2}$ in equilibrium with calcite. Phase boundaries between Al-bearing minerals are shown as solid lines. Saturation surfaces for stoichiometric diposide, talc, wollastonite, and tremolite are depicted as dotted lines. Two sets of phase boundaries involving clinochlore are depicted in figure 12: one for endmember clinochlore ($a_{clinochlore}$ = 1; solid lines) and one corresponding to $a_{clinochlore}$ = 0.0068 (dash-dot-dot lines), the activity of clinochlore in sample 94-94 (table 2) assuming ideal mixing (Holland, Baker, and Powell, 1998). Prehnite is not depicted on the diagram as the thermodynamic properties reported for this phase in Johnson, Oeklers, and Helgeson (1992) imply that it is stable relative to all Ca-zeolites, conflicting with experimental and field evidence indicating that Ca-zeolites are stable relative to prehnite at this temperature and pressure. Trends A and B are discussed in the text.

sumed Mg, causing the value of log $[(a_{Ca^{+2}})/(a_{Mg^{+2}})]$ to increase as inferred above from natural parageneses.

Fluid compositions in local equilibrium with Stage II mineral assemblages were predicted using Version 8 of the computer code EQ3NR (Wolery, 1991) assuming heterogeneous equilibrium at 100°C, 500 bar between clinochlore, stilbite, quartz, and albite. Additional constraints were provided by fixing the concentration of $Cl^-$ to 0.001 (representative concentration in meteoric-water dominated geothermal systems in Ice-

land; Arnórsson, Sigurdsson, and Svavarsson, 1982; Arnórsson, Gunnlaugsson, and Svavarson, 1983) and assuming that the activity of $Ca^{+2}$ was constrained by the absence of grossular and paragonite in the assemblage (fig. 14). Resulting fluid compositions were basic (pH 8.78-9.20) with activities of $Ca^{+2}$ ($\log a_{Ca^{+2}} = -5.59$ to $-4.99$) that are 2 to 3.5 orders of magnitude higher than the activity of $Mg^{+2}$ ($\log a_{Mg^{+2}} = -8.44$ to $-7.89$). Calculated values of $\log [(a_{Ca^{+2}})/(a_{Mg^{+2}})]$ agree well with values computed using compositions of Icelandic geothermal fluids at temperatures near 100°C (Arnórsson, Sigurdsson, and Svavarsson, 1982; Arnórsson, Gunnlaugsson, and Svavarson, 1983). The absence of calcite during Stage II requires that $\log f_{CO2}$ was less than $-2.5$ bars (fig. 14).

*Porosity evolution.*–Hydrogeochemical modeling of reactive fluid transport (Rose, 1995; Manning, Ingebritsen, and Bird, 1993) and field observations (Manning and Bird, 1991, 1995; Robert and Goffé, 1993; Bevins, Rowbotham, and Robinson, 1991; Schmidt, 1990; Schmidt and Robinson, 1997) demonstrate the importance of porosity ($\Phi$) and permeability (k) in controlling mineral parageneses in low-grade metabasalts. In particular, the magnitude of k influences the extent and distribution of chemical alteration during hydrothermal and metamorphic processes (Norton, 1988; Rose, 1995). In regions of large $\Phi$ and k, high fluid fluxes promote disequilibrium conditions that can influence the locations of mineral isograds (Lasaga and Rye, 1993; Lasaga, 1989; Bolton, Lasaga, and Rye, 1999; Dewers and Ortoleva, 1990) and promote metastable mineral formation (Steefel and Van Cappellen, 1990; Steefel and Lasaga, 1994). Consequently, measurements of $\Phi$ and k are critical for modeling mineralogical alteration during fluid flow (Norton, 1988; Norton and Knapp, 1977). In lavas, these properties are controlled by complex sequences of pore forming events (for example, degassing of the lava to form vesicles during eruption, brittle deformation after extrusion, dissolution of primary minerals during metasomatism) and reduction of $\Phi$ through mineral precipitations. Typical laboratory measurements of $\Phi$ (Norton and Knapp, 1977) in altered rocks reflect the cumulative effects of these processes. Laboratory measurements on altered rocks typically underestimate k during active stages of hydrothermal and metamorphic flow systems because much of the $\Phi$ is occluded by secondary minerals (Norton, 1988). Although laboratory measurements of initial $\Phi$ on unaltered rocks or outcrop measurements of pore abundance (such as those conducted in this study) can in part mitigate these problems, it is clear that $\Phi$ and k change dramatically with time (generally decreasing) during progressive infilling of pore spaces during mineralogical alteration (Ague, 1995). In addition, systematic decreases in k with depth in the crust (Manning and Ingebritsen, 1999) can at least partially be attributed to mineral precipitation. Generation of secondary $\Phi$ associated with mineral dissolution during alteration (Ortoleva and others, 1987) also complicates assessment of $\Phi$ and k at various stages in the alteration history of crustal rocks.

The data in tables 7 and 8 provide quantitative estimates of the amount of porosity created during volcanism and brittle deformation ($\Phi_1^*$ and $\Phi_2^*$, respectively) and of the amount of $\Phi_1^*$ destroyed through mineral precipitation. These data are summarized in figure 15, which depicts the evolution of $\Phi$ at Teigarhorn as a function of the three stages in mineral paragenesis. Two main pore forming events influenced the lavas at Teigarhorn: creation of primary $\Phi$ during extrusion and solidification of the lavas and brittle deformation during dike emplacement. Vesiculation of the lavas resulted in a heterogeneous distribution of $\Phi_1^*$, with flow tops having as much as 22 percent $\Phi_1^*$ and flow centers being essentially non-porous. Sporadic development of Stage I alteration decreased the value of $\Phi$ by ~8 percent on average. Precipitation of Stage II C/S during burial resulted in a loss of an additional 40 percent of $\Phi$. Stage II zeolites filled most of the remaining volume of $\Phi_1^*$. Development of Stage III alteration required addition of 3 to 11 percent total porosity ($\Phi_2^*$) through brittle deformation. Quantitative measurements of the degree of filling of $\Phi_2^*$ by Stage III minerals were not conducted. However, outcrop observations

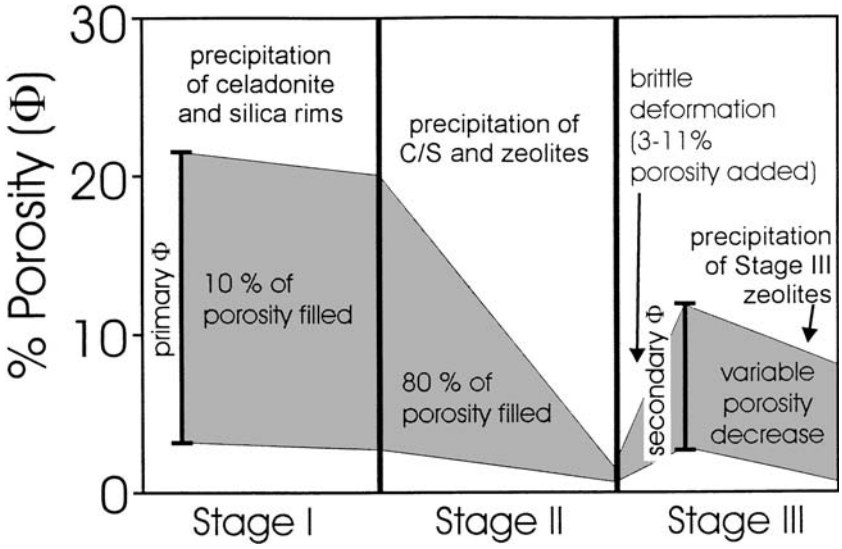


Fig. 15. Variation of bulk porosity (percent) in lavas at Teigarhorn as a function of paragenetic stage (based on the measurements in tables 7 and 8). Time elapsed after eruption increases to the right. Vertical brackets illustrate the ranges in total primary and secondary porosity determined by outcrop and thin section measurements. The gray region illustrates changes in the range of bulk porosity values realized through geologic time, with the relative height and absolute position of the boundaries of this region illustrating the variation in and magnitude of porosity.

suggest that the percent of Φ occluded by mineral precipitation during Stage III was smaller than that in Stage II as evidenced by the abundant open cavities remaining in breccias and fractures that host museum-grade zeolite, quartz, and Iceland spar crystals.

The textures and extent of infilling of primary pore spaces during Stages I and II suggest that although Φ decreased during alteration, the matrix of the lavas was sufficiently permeable to permit transport of chemical components necessary for precipitation of observed mineral assemblages. As noted above, mass transfer must have occurred from the matrix of the lavas to primary pore spaces. This apparently was true even after pore walls were coated with Stage I silica and celadonite and Stage II C/S. With the exception of scoreaceous zones, where connections between pore spaces are readily observable, much of the Stage I and II pore filling occurred in effectively isolated vesicles. Vesicles hosting Stage II minerals were thus only partially sealed by precipitation of Stage I minerals and Stage II C/S. The nearly complete infilling of $\Phi_1^*$ during Stage II was particularly acute because of the large molar volumes of zeolites and smectites. Subsequent alteration was limited by the lack of pore space for storage and migration of fluids, except where brittle deformation locally increased Φ, resulting in Stage III alteration.

Although Φ was larger in flow tops at the onset of Stage II than in Stage III (table 7), fractures conducting fluid flow during Stage III are often laterally continuous in outcrop for as much as 10 m and associated with irregular porous metasomatized aureoles (figs. 10, 11C and D). Thus, k during Stage III was probably much greater initially than in porous zones occupied by Stage I and II minerals, despite lower values of Φ (table 7). The extensive metasomatism producing the vuggy $SiO_2$-rich zones near Stage III pores was likely a consequence of high water/rock ratios possible in large, conductive fractures. Late precipitation of zeolites closed the fractures, resulting in a decrease of both Φ and k. The duration of convective fluid and heat transport during Stage III was probably limited by declining k due to fracture filling.

## CONCLUDING REMARKS

The mineral parageneses observed in eastern Iceland and other low-grade metabasalt localities often result from multiple stages of alteration that can be difficult to distinguish. However, as shown in figure 13, the textural and mineralogical signatures of low-grade metamorphism can be interpreted by relatively simple paragenetic schemes that account for the tectonic history of the lavas. It is also readily apparent that mineral precipitation and tectonic events accompanying the paragenetic stages depicted in figure 13 profoundly influence the hydrogeologic properties of basaltic crust (fig. 15).

An example of the importance of petrotectonic interpretations of zeolite-facies mineral parageneses is the "zone of abundant zeolites," described by Walker (1960b) as the deepest exposed mineral zone developed in non-olivine normative tholeiitic lavas in eastern Iceland. The assemblage described by Walker (1960b) in this zone ("magnificent specimens" of heulandite, stilbite, scolecite, epistilbite) is similar to the integrated mineralogy of Stage II and III alteration found at Teigarhorn, which Walker (1960b) cited as a type locality for the "zone of abundant zeolites." Inspection of figures 3 and 4 in Walker (1960b) suggests that the vertical extent of the "zone of abundant zeolites" is correlated to dike distribution along the northern shore of Berufjördur just as the distribution of Stage III alteration at Teigarhorn is associated with dikes. Based on these comparisons, it appears that the "zone of abundant zeolites" reported by Walker (1960b) represents hydrothermal aureoles around dike swarms and is not a signature of burial metamorphism.

## ACKNOWLEDGMENTS

The authors would like to thank Herbert Hjörleifsson for graciously granting us access to the outcrops at Teigarhorn, Elsa Thórey Eysteinsdóttir, Gunnlaugur Fridbjarnarson, and Obba, Óskar, and Berta Sandholt for friendship and hospitality, and the citizens of Djúpivogur for accommodating us during our work at Teigarhorn. Anne Dyreborg assisted with the fluid inclusion analyses. This work was funded by the Shell and McGee Funds at Stanford University, the Geological Society of America, the Icelandic Student Innovation Fund, the Petroleum Research Fund (grant ACS-PRF 31742-AC2 to DKB), and graduate fellowships from the United States National Science Foundation and Environmental Protection Agency (to PSN). Discussions with L. Heister, A. Stefánsson, and S. Jakobsson and reviews by J. Liou and P. Schiffman contributed significantly to our interpretations.

## REFERENCES

Ague, J. J., 1995, Deep crustal growth of quartz, kyanite, and garnet into large-aperture, fluid-filled fractures, north-eastern Connecticut, USA: Journal of Metamorphic Geology, v. 13, p. 299-314.

Alberti, A., Pongiluppi, D., and Vezzalini, G., 1982, The Crystal Chemistry of Natrolite, Mesolite and Scolecite: Neues Jarbuch fur Mineralogie, Abhandlungen, v. 143, p. 231-248.

Alt, J. C., 1999, Very low-grade hydrothermal metamorphism of basic igenous rocks, *in* Frey, M., and Robinson, D., editors, Low Grade Metamorphism: Oxford, Blackwell Science Ltd., p. 169-201.

Arnórsson, S., Gunnlaugsson, E., and Svavarsson, H., 1983, The chemistry of geothermal waters in Iceland; II, Mineral equilibria and independent variables controlling water compositions: Geochemica et Cosmochimica Acta, v. 47, p. 547-566.

Arnórsson, S., Sigurdsson, S., and Svavarsson, H., 1982, The chemistry of geothermal waters in Iceland; I, Calculation of aqueous speciation from 0 degrees to 370 degrees C: Geochemica et Cosmochimica Acta, v. 46, p. 1513-1532.

Bailey, S. W., 1988, Chlorites: structures and crystal chemistry, *In* Bailey, S. W., editor, Hydrous Phyllosilicates: Mineralogical Society of America Reviews in Mineralogy, v. 19, p. 347-403.

Bauer, J., and Hrichová, R., 1962, Ptilolite (mordenite) from Teigarhorn, Iceland: Sbornik Vysoke Skoly Chemicko-Technologicke V Praze, Mineralogie, v. 6, p. 27-36.

Bellanca, A., 1940, Piezoelettricita e legge di geminazione della scolecite: Societa de Scienze Naturali Ed Economiche di Palermo. Bollettino, v. 22, p. 11-18.

Betz, V., 1981, Famous mineral localities; zeolites from Iceland and the Faeroes: The Mineralogical Record, v. 12, p. 5-26.

Bevins, R. E., Robinson, D., and Rowbotham, G., 1991, Compositional variations in mafic phyllosilicates from regional low-grade metabasites and application of the chlorite geothermometer: Journal of Metamorphic Geology, v. 9, p. 711-721.

Bevins, R. E., Rowbotham, G., and Robinson, D., 1991, Zeolite to prehnite-pumpellyite facies metamorphism of the late Proterozoic Zig-Zag Dal Basalt Formation, eastern North Greenland: Lithios, v. 27, p. 155-165.
Blake, D. H., 1970, Geology of Alftafjördur volcano, a Tertiary volcanic centre in south-eastern Iceland: Visindafelag Islendinga [Rit], v. 2, p. 43-63.
Bolton, E. W., Lasaga, A. C., and Rye, D. M., 1999, Long-term flow/chemistry feedback in a porous medium with heterogeneous permeability: kinetic control of dissolution and precipitation: American Journal of Science, v. 299, p. 1-68.
Buckley, H. A., Bevan, J. C., Brown, K. M., and Johnson, R., 1978, Glauconite and celadonite: Two separate mineral species: Mineralogical Magazine, v. 42, p. 373-382.
Cathelineau, M., 1988, Cation site occupancy in chlorites and illites as a function of temperature: Clay Minerals, v. 23, p. 471-485.
Cathelineau, M., and Nieva, D., 1985, A chlorite solid solution geothermometer. The Los Azulfres geothermal system (Mexico): Contributions to Mineralogy and Petrology, v. 91, p. 235-244.
Chayes, F., 1956, Petrographic model analysis: an elementary statistical appraisal: New York, John Wiley and Sons, 113 p.
Christiansen, F. G., Boesen, A., Bojesen-Koefoed, J., Dallhoff, F., Dam, G., Neuhoff, P. S., Pedersen, A. K., Pedersen, G. K., Stannius, L. S., and Zinck-Joergensen, K., 1999, Petroleum geological activities onshore West Greenland in 1997: Geology of Greenland Survey Bulletin, v. 180, p. 10-17.
Christensen, N. I., and Wilkens, R. H., 1982, Seismic properties, density, and composition of the Icelandic crust near Reydarfjördur: Journal of Geophysical Research, v. 87, p. 6389-6395.
Dewers, T., and Ortoleva, P., 1990, Geochemical self-organization III: Mechano-chemical model of metamorphic differentiation: American Journal of Science, v. 290, p. 473-521.
Flóvenz, O. G., and Sæmundsson, K., 1993, Heat flow and geothermal processes in Iceland: Tectonophysics, v. 225, p. 123-138.
Flower, M. F. J., Pritchard, R. G., Brem, G., Cann, J. R., Delaney, J., Emmerman, R., Gibson, I. L., Oakley, P. J., Robinson, P. T., and Schmincke, H.-U., 1982, Chemical stratigraphy, Iceland Research Drilling Project, Reydarfjordur, eastern Iceland: Journal of Geophysical Research, v. 87, p. 6489-6610.
Galli, R., and Rinaldi, R., 1974, The Crystal Chemistry of Epistilbites: American Mineralogist, v. 59, p. 1055-1061.
Ghiara, M. R., Franco, E., Petti, C., Stanzione, D., and Valentino, G.M., 1993, Hydrothermal interaction between basaltic glass, deionized water and seawater: Chemical Geology, v. 104, p. 125-138.
Gíslason, S. R., and Arnórsson, S., 1993, Dissolution of primary basaltic minerals in natural waters: saturation state and kinetics: Chemical Geology, v. 105, p. 117-135.
Gíslason, S. R., Arnórsson, S., and Ármannsson, H., 1996, Chemical weathering of basalt in Southwest Iceland; effects of runoff, age of rocks and vegetative/glacial cover: American Journal of Science, v. 296, p. 837-907.
Gíslason, S. R., and Eugster, H. P., 1987a, Meteoric water-basalt interactions. I: A laboratory study: Geochemica et Cosmochimica Acta, v. 51, p. 2827-2840.
——— 1987b, Meteroric water-basalt interactions. II: A field study in NE Iceland: Geochemica et Cosmochimica Acta, v. 51, p. 2841-2855.
Gíslason, S. R., Veblen, D. R., and Livi, K. J. T., 1993, Experimental meteoric water-basalt interactions: Characterization and interpretation of alteration products: Geochimica et Cosmochimica Acta, v. 57, p. 1459-1471.
Grant, J. A., 1982, The Isocon Diagram—A Simple Solution to Gresens' Equation for Metasomatic Alteration: Economic Geology, v. 81, p. 1976-1982.
Gústafsson, L. E., 1992, Geology and petrography of the Dyrfjöll central volcano, eastern Iceland: Berliner Geowissenschaftliche Abhandlungen, v. 138, p. 1-101.
Güven, N., 1988, Smectites, *In* Bailey, S. W., editor, Hydrous Phyllosilicates: Mineralogical Society of America Reviews in Mineralogy, v. 19, p. 497-559.
Heister, L. E., ms, 1997, The petrogenesis of Tertiary phonolitic volcanism Gronau West Nunatak, East Greenland: M.S. thesis, Arizona State University, Tempe, Arizona, 12 p.
Holland, T., Baker, J., and Powell, R., 1998, Mixing properties and activity-composition relationships of chlorites in the system MgO-FeO-$Al_2O_3$-$SiO_2$-$H_2O$: European Journal of Mineralogy, v. 10, p. 395-406.
Jóhannesson, H., and Sæmundsson, K., 1989, Geological Map of Iceland. 1:500000. Bedrock Geology: Reykjavik, Iceland, Icelandic Museum of Natural History and Iceland Geodetic Survey, 1 sheet.
Johnson, J. W., Oelkers, E. H., and Helgeson, H. C., 1992, SUPCRT92: Software package for calculating the standard molar thermodynamic properties of minerals, gases, aqueous species, and reactions among them as functions of temperature and pressure: Computers in Geoscience, v. 18, p. 899-947.
Jørgensen, O., 1984, Zeolite zones in the basaltic lavas of the Faeroe Islands. *In* The deep drilling project 1980-1981 in the Faeroe Islands: Annales Societatia Scientarum Faroensis, Supplementum, v. 9, p. 71-91.
Kristjánsson, L., Gudmundsson, A., and Haraldsson, H., 1995, Stratigraphy and paleomagnetism of a 3-km-thick Miocene lava pile in the Mjoifjordur area, eastern Iceland: Geologische Rundschau, v. 84, p. 813-830.
Kristmannsdóttir, H., 1979, Alteration of basaltic rocks by hydrothermal activity at 100-300°C, *in* Mortland, M., and Farmer, V., editors, Developments in Sedimentology, v. 27: Amsterdam, Elsevier, p. 359-367.
Kristmannsdóttir, H., and Tómasson, J., 1978, Zeolite zones in geothermal areas in Iceland, *in* Sand, L. B., and Mumpton, F. A., editors, Natural Zeolites: Oxford, Pergamon Press Ltd., p. 277-284.
Lasaga, A. C., 1986, Metamorphic reaction rate laws and the development of isograds: Mineralogical Magazine, v. 50, p. 359-373.
——— 1989, Fluid flow and chemical reaction kinetics in metamorphic systems: a new simple model: Earth and Planetary Science Letters, v. 94, p. 417-424.

Lasaga, A. C., and Rye, D. M., 1993, Fluid flow and chemical reaction kinetics in metamorphic systems: American Journal of Science, v. 293, p. 361-404.
Liou, J. G., Seki, Y. S., Guillemette, R. N., and Sakai, H. U., 1985, Compositions and parageneses of secondary minerals in the Onikobe geothermal system, Japan: Chemical Geology, v. 49, p. 1-20.
Manning, C. E., and Bird, D. K., 1991, Porosity evolution and fluid flow in the basalts of the Skaergaard magma-hydrothermal system, East Greenland: American Journal of Science, v. 291, p. 201-257.
——— 1995, Porosity, permeability, and basalt metamorphism, *in* Schiffman, P., and Day, H. W., editors, Low-Grade Metamorphism of Mafic Rocks: Geological Society of America Special Paper 296, p. 123-140.
Manning, C. E., and Ingebritsen, S. E., 1999, Permeability of the continental crust: Implications of geothermal data and metamorphic systems: Reviews in Geophysics, v. 37, p. 127-150.
Manning, C. E., Ingebritsen, S. E., and Bird, D. K., 1993, Missing mineral zones in contact metamorphosed basalts: American Journal of Science, v. 293, p. 894-938.
Mehegan, J. M., Robinson, P. T., and Delaney, J. R., 1982, Secondary mineralization and hydrothermal alteration in the Reydarfjördur drill core, eastern Iceland: Journal of Geophysical Research, v. 87, p. 6511-6524.
Murata, K. J., Formoso, M. L. L., and Roisenberg, A., 1987, Distribution of zeolites in lavas of southeastern Parana Basin, state of Rio Grande do Sul, Brazil: Journal of Geology, v. 95, p. 455-467.
Neuhoff, P. S., Watt, W. S., Bird, D. K., and Pedersen, A. K., 1997, Timing and Structural Relations of Regional Zeolite Zones in Basalts of the East Greenland Continental Margin: Geology, v. 25, p. 803-806.
Norton, D., 1988, Metasomatism and permeability: American Journal of Science, v. 288, p. 604-618.
Norton, D., and Knapp, R., 1977, Transport phenomena in hydrothermal systems: The nature of porosity: American Journal of Science, v. 277, p. 913-936.
Odin, G. S., Desprairies, A., Fullagar, P. D., Bellon, H., Decarreau, A., Froehlich, F., and Zelvelder, M., 1988, Nature and geological significance of celadonite, *in* Odin, G. S., editor, Green marine clays; oolitic ironstone facies, verdine facies, glaucony facies and celadonite-bearing facies; a comparative study: Developments in Sedimentology, v. 45, p. 337-398.
Ortoleva, P., Chadam, J., Merino, E., and Sen, A., 1987, Geochemical self-organization II: The reactive-infiltration instability: American Journal of Science, v. 287, p. 1008-1040.
Oxburgh, E. R., and Agrell, S. O., 1982, Thermal conductivity and temperature structure of the Reydarfjordur borehole: Journal of Geophysical Research, v. 87, p. 6423-6428.
Pálmason, G., 1973, Crustal rifting, and related thermo-mechanical processes in the lithosphere beneath Iceland: Geologische Rundschau, v. 70, p. 244-260.
Passaglia, E., 1975, The crystal chemistry of mordenites: Contributions to Mineralogy and Petrology, v. 50, p. 65-77.
Passaglia, E., Galli, E., Leoni, L., and Rossi, G., 1978, The Crystal Chemistry of Stilbites and Stellerites: Bulletin de Mineralogie, v. 101, p. 368-375.
Ragnarsdóttir, K. V., 1993, Dissolution kinetics of heulandite at pH 2-12 and 25°C: Geochimica et Cosmochimica Acta, v. 57, p. 2439-2449.
Reynolds, R. C. J., 1988, Interstratified clay minerals, *in* Brindley, G. W., and Brown, G., editors, Crystal Structures of Clay Minerals and Their X-ray Identification: London, Mineralogical Society, p. 249-304.
Robert, C., and Goffé, B., 1993, Zeolitization of basalts in subaqueous freshwater settings: Field observations and experimental study: Geochimica et Cosmochimica Acta, v. 57, p. 3597-3612.
Robinson, D., and Bevins, R. E., 1999, Patterns of regional low-grade metamorphism in metabasites, *in* Frey, M., and Robinson, D., editors, Low Grade Metamorphism: Oxford, Blackwell Science Ltd., p. 143-168.
Robinson, D., Bevins, R. E., and Rowbotham, G., 1993, The characterization of mafic phyllosilicates in low-grade metabasalts from eastern North Greenland: American Mineralogist, v. 78, p. 377-390.
Robinson, P. T., Mehegan, J., Gibson, I. L., and Schmincke, H.-U., 1982, Lithology and structure of the volcanic sequence in eastern Iceland: Journal of Geophysical Research, v. 87, p. 6429-6436.
Rose, N. M., 1995, Geochemical consequences of fluid flow in porous basaltic crust containing permeability contrasts: Geochemica et Cosmochimica Acta, v. 59, p. 4381-4392.
Sæmundsson, K., 1979, Outline of the geology of Iceland: Jökull, v. 29, p. 7-28.
Schiffman, P., and Fridleifsson, G. Ó., 1991, The smectite-chlorite transition in drillhole NJ-15, Nesjavellir geothermal field, Iceland: XRD, BSE and electron microprobe investigations: Journal of Metamorphic Geology, v. 9, p. 679-696.
Schmidt, S. Th., 1990, Alteration under conditions of burial metamorphism in the North Shore Volcanic Group, Minnesota–Mineralogical and geochemical zonation: Heidelberger Geowissenschaftliche Abhandlungen, v. 41, 309 pp.
Schmidt, S. Th., and Robinson, D., 1997, Metamorphic grade and porosity and permeability controls on mafic phyllosilicate distributions in a regional zeolite to greenschist facies transition of the North Shore Volcanic Group, Minnesota: Geological Society of America Bulletin, v. 109, p. 683-697.
Seki, Y., Liou, J. G., Guillemette, R., Sakai, H., Oki, Y., Hirano, T., and Onuki, H., 1983, Investigation of geothermal systems in Japan. I. Onikobe Geothermal Area: Saitama University 3, Hydroscience and Geotechnology Laboratory, Memoir, 206 pp.
Shau, Y.-H., and Peacor, D. R., 1992, Phyllosilicates in hydrothermally altered basalts from DSDP Hole 504B, leg 83_A TEM and AEM study: Contributions to Mineralogy and Petrology, v. 112, p. 119-133.
Slaughter, M., and Kane, W. T., 1969, The crystal structure of a disordered epistilbite: Zeitschrift für Kristallographie, v. 130, p. 68-87.
Steefel, C. I., and Lasaga, A. C., 1994, A coupled model for transport of multiple chemical species and kinetic precipitation/dissolution reactions with applications to reactive flow in single phase hydrothermal systems: American Journal of Science, v. 294, p. 529-592.

Steefel, C. I., and Van Cappellen, P., 1990, A new kinetic approach to modeling water-rock interaction: the role of nucleation, precursors, and Ostwald ripening: Geochimica et Cosmochimica Acta, v. 54, p. 2657-2677.

Sukheswala, R. N., Avasia, R. K., and Gangopadhyay, M., 1974, Zeolites and associated secondary minerals in the Deccan Traps of Western India: Mineralogical Magazine, v. 39, p. 658-671.

Tingle, T. N., Neuhoff, P. S., Ostergren, J. D., Jones, R. E., and Donovan, J. J., 1996, The effect of 'missing' (unanalyzed) oxygen on quantitative electron microprobe microanalysis of hydrous silicate and oxide minerals: Geological Society of America, Abstracts with Programs, v. 28, p. A-212.

Walker, G. P. L., 1951, The amygdale minerals in the Tertiary lavas of Ireland. I. The distribution of chabazite habits and zeolites in the Garron plateau area, County Antrim: Mineralogy Magazine, v. 29, p. 773-791.

——— 1959, Geology of the Reyoarfjörour area, eastern Iceland. The Quarterly Journal of the Geological Society of London, v. 114, p. 367-393.

——— 1960a, The amygdale minerals of the Tertiary lavas of Ireland. III. Regional distribution: Mineralogical Magazine, v. 32, p. 515-528.

——— 1960b, Zeolite zones and dike distribution in relation to the structure of the basalts of eastern Iceland: Journal of Geology, v. 68, p. 515-528.

——— 1962, Tertiary welded tuffs in eastern Iceland: The Quarterly Journal of the Geological Society of London, v. 118, p. 275-293.

——— 1963, The Breiddalur central volcano, eastern Iceland [with discussion]: The Quarterly Journal of the Geological Society of London, v. 119, p. 29-63.

——— 1974, The structure of eastern Iceland: in Kristjánsson, l., editor, Geodynamics of Iceland and the North Atlantic Area: Reykjavik, Iceland, NATO Advanced Study Institute, p. 177-188.

Watkins, N. D., and Walker, G. P., L., 1977, Magnetostratigraphy of eastern Iceland: American Journal of Science, v. 277, p. 513-584.

Wolery, T. J., 1991, EQ3NR. A computer program for geochemical aqueous speciation solubility calculations: Theoretical manual, user's guide and related documentation (Version 7.0). Livermore, California, Lawrence Livermore National Laboratory report UCRL-MA-110662 Pt III.

Wood, D. A., 1976, Elemental Mobility during Zeolite Facies Metamorphism of the Tertiary Basalts of Eastern Iceland: Contributions to Mineralogy and Petrology, v. 55, p. 241-254.

——— 1977, Major and trace element variations in the Tertiary lavas of eastern Iceland and their significance with respect to the Iceland geochemical anomaly: Journal of Petrology, v. 19, p. 393-436.